POLITECNICO DI TORINO

Corso di Laurea Magistrale
in Ingegneria Energetica e Nucleare

Tesi di Laurea Magistrale

Simulation and analysis of hydrogen networks for heating applications: a case study in the Netherlands

Relatori:

prof. Pierluigi Leone

Carla Robledo

Co-relatori:

Marco Cavana

Enrico Vaccariello

Candidata:

Valeria Di Francesco

Luglio 2019

A mamma e papà

Abstract

La tesi proposta vuole studiare una rete di distribuzione di idrogeno realizzata nel campus dell'Università Tecnica di Delft, nei Paesi Bassi. Essa verrà utilizzata inizialmente per alimentare la caldaia di una piccola abitazione, chiamata Prèt-à-loger, frutto della partecipazione alla competizione studentesca internazionale Solar Decathlon 2014. La simulazione è il risultato dell'applicazione di un modello transitorio isotermo sviluppato in Matlab al caso specifico, considerando sia la connessione con la singola abitazione, che i futuri sviluppi della rete. Nell'ipotesi di produzione di idrogeno in situ attraverso un elettrolizzatore, vengono realizzate delle analisi energetiche sulle possibilità di produzione del gas usando l'energia prodotta dai pannelli fotovoltaici installati nell'area. Alla luce delle simulazioni e delle analisi, si vaglia la possibilità di realizzare un accumulo stagionale di idrogeno al fine di massimizzare l'autoconsumo di energia rinnovabile.

The thesis aims at studying a hydrogen distribution network built in the campus of Technical University of Delft, in the Netherlands. It will be used in the immediate future to feed a boiler of a small house, the Prèt-à-loger, a prototype of the project made for the international student competition Solar Decathlon 2014. The simulation is the result of the application of an isothermal transient model developed in Matlab to the case study, considering both the single connection to the house, and the future expansion of the network. It is evaluated the possibility of using an electrolyser to produce the hydrogen needed on site, exploiting the energy produced by the photovoltaic panels installed in the area. It is then assessed the feasibility of using the hydrogen for a seasonal storage to maximize the self-consumption of renewable energy.

Summary

Introduction

Hydrogen's use in the energy sector is experiencing now an unprecedented moment of business and political drive, with a number of projects and policies growing rapidly around the world. By mid-2019, the number of actions to foster the spread of hydrogen development and use was around 50, all over the world, most of them oriented to the transport sector, and to heat and power production for buildings [1]. In particular, European Union published a long-term strategy for decarbonisation that includes hydrogen development and set up a "Hydrogen Energy Network" to allow the transfer of knowledge and practices among the EU member states. Italy helped to overcome the limits to hydrogen exploitation increasing the allowable delivery pressure of refuelling stations, and improving safety, economic and social aspects. The Netherlands included hydrogen in the Dutch Climate Agreement, and published a hydrogen roadmap, setting some ambitious goals for hydrogen deployment. The actions planned to push hydrogen development involve several sectors related to energy like transport, electricity, heating, but also industry, being a fundamental element for several production processes. In fact, hydrogen is today mainly used to produce ammonia (e.g. ammonium nitrate for fertilizers), and in refining processes (hydrocracking), but it can be used to produce other chemicals like methanol, synthetic methane, synthetic fuels in general. The high diversification of end-uses makes the hydrogen a crucial gas for sector coupling.

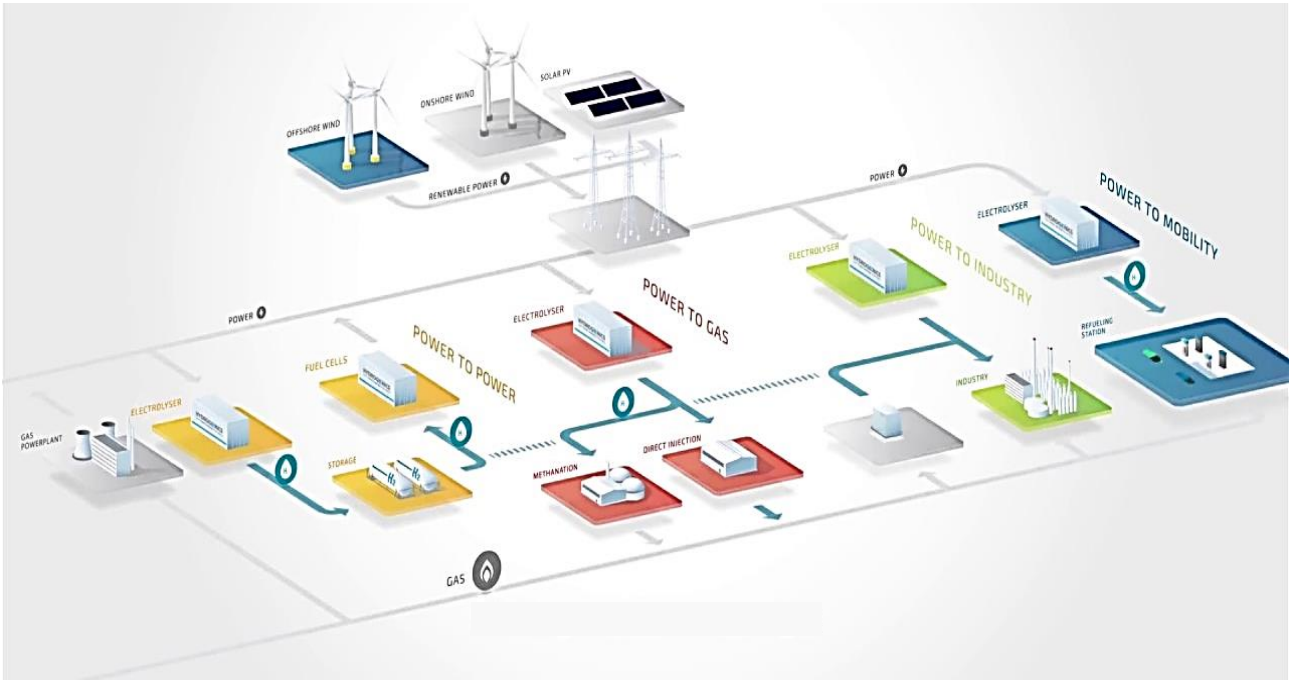

Figure 1 Picture of sector coupling through hydrogen by the company Hydrogenics.[2]

The production of "green" hydrogen from photovoltaic and wind energy allows to implement a so-called Power-to-X system: standing for the direction of the energy conversion, this term refers to all type of conversion of electricity to other energy carriers or chemicals. In fig.1 a schematic explanation of the possibilities involving hydrogen gas is shown. The common element of the configurations is the electrolyser: an electrochemical device that is able to split water molecules by electricity consumption. The gas can be stored in pressurized tanks when the power produced by renewables is not needed, and then re-converted into water to produce power thanks to fuel cells when the demand rises. Hydrogen could be used in the methanation process to produce synthetic methane, or other chemicals, in a power-to-gas solution, or directly injected into the gas grid. It can be used as feedstock by industries, or it can be destined to refuelling stations for Fuel Cells Electric Vehicles. Similarly to electricity, hydrogen is an energy carrier, not an energy source, so it is subjected to energy losses during the process of production, transportation and reconversion to water, determining in some cases the delivery of power from fuel cells with an energy content that is 30% of the initial electricity input [1].

The growing interest for hydrogen implementation in clean energy systems comes mainly from two elements: the possibility of using it without direct emissions of air pollutants or green-house gases, and the diversity of low-carbon energy sources that can be used to obtain it, i.e. renewables, nuclear energy and biomass. For instance, hydrogen can be burnt in dedicated furnaces, having water as only product of the reaction, to get heat, either it can be used in fuel cells, to directly produce electricity. It can be obtained from electrolysers powered by renewable energy, working as a storage medium, or by nuclear energy, more reliable in terms of availability.

In the Netherlands, forward-looking companies have been investing in research and development of hydrogen technologies and infrastructure in the last ten years, especially the natural gas grid operators.

This work aims at finding the answers to the following questions:

What is the hydrogen network behaviour of The Green Village? Can the hydrogen be produced on site to satisfy the Prèt-à-loger house heating demand? Is the network able to work as a gas storage thanks to line packing?

In the first chapter of the dissertation, after a better explanation of why hydrogen is so important for the energy sector, the projects in development and the legislation in the Netherlands and in Italy will be revised, looking deeper into the legislative situations of the countries when it comes to

hydrogen projects. Chapter 2 will be dedicated to the case study presentation: in the Green Village, located in the campus of Technical University of Delft, the Prèt-à-loger house will be connected to a hydrogen network. The description in depth of the thermodynamics and the fluid-dynamics of the problem is developed in Chapter 3, together with the model characteristics. A study on the equations of state for real gases to be used for hydrogen is conducted, to select the best formula to implement in the model for the case analysed. In Chapter 4, the heating consumption loads of the Prèt-à-loger are profiled, to get all the inputs for the model, and the photovoltaic power production is analysed to evaluate the possibility of introducing electrolysers for hydrogen production on site. Then, the model is run, and the simulations are shown in the Chapter 5, for a base case, for the real case, and for a hypothetical case with more consumers. Finally, the conclusions are drawn in Chapter 6.

1. Hydrogen roadmap

Despite the possibility to obtain it from renewable sources, or from nuclear energy, today hydrogen is mainly supplied from fossil fuels, with 6% of global natural gas and 2% of global coal used for H_2 production. As a consequence, its production is responsible for the emissions of 830 Mt/y of CO_2, equivalent to the carbon dioxide emitted every year by United Kingdom and Indonesia combined. Hydrogen can be used in a wide range of applications, it is today mainly used for refining processes, for ammonia production, and in smaller part, for methanol and direct reduced iron steel production. Its global annual demand has been rising since 1975, from 18 up to 70 million tonnes (Mt/yr) in 2018 [1]. The boost of hydrogen clean production and consumption can therefore have a huge impact on the greenhouse gases emissions reduction and on the improvement of the air quality, thanks to the avoided carbon dioxide and particulate emissions. Moreover, it can help to make the contribution of renewable energy more effective, as they become cheaper and cheaper. In fact, the cost of renewable energy technologies is decreasing, so their share in energy production is expected to grow in the future, posing some challenges for the power grid. Because of the high intermittency and unpredictability of renewable sources like wind and sun, the balancing between production and consumption is harder to guarantee, and not always possible, forcing grid operators to curtail the energy from renewables when it exceeds the demand. Hydrogen production can represent a valid help to solve the mismatch, and to increase the renewable energy deployment. The Netherlands are one of the countries whose companies are investing the most in hydrogen, fostered by forward-thinking policies.

1.1 The Netherlands

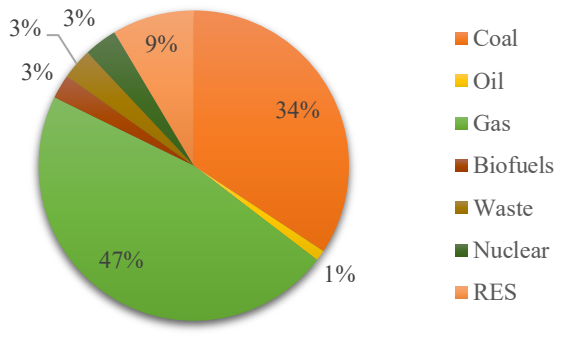

Figure 2 Electricity production by sources in the Netherlands. Elaboration of IEA data [4].

The scope of this research is tailored on The Green Village hydrogen network designed and installed by the company Stedin, a regional gas and electricity grids manager in South Holland. In collaboration with other Dutch companies, like Alliander and Enexis Groep, and universities (TU Delft included), Stedin signed the Manifest Hydrogen Coalition, a recent initiative of Greenpeace Netherlands that involves different parties whose purpose is to come together to sustain the importance of green hydrogen

in the energy transition [3]. The twenty-three organizations that form the Hydrogen Coalition agree that hydrogen can be a valid long-term storage solution for renewable energy, allowing the reduction of CO_2 emitting technologies. At the moment, the "green" hydrogen, the one obtained from renewable energy, is a more expensive alternative with respect to "grey" hydrogen, which is the one obtained from fossil fuels, or "blue" hydrogen, where the source is the same, but the carbon dioxide produced is captured. That is why it is fundamental to increase the renewable energy capacity, through large off-shore wind power plants and distributed generation, reducing the electricity costs, and to increase the number of electrolysers, the devices that make possible the production of green hydrogen [4]. These parties joined to ask to the government to extend the Wind@Sea budget to large electrolysis plants and H_2 networks development, in order to increase up to 3-4 GW the electrolysis capacity within 2030 and as a consequence to bring down the cost of hydrogen that is not produced from steam methane reforming, to around 3€/kg by the same year [4]. This is just one of the several commitments that Netherlands has made for the energy transition: 100 projects involving hydrogen were counted on short and long timeline [5]. Among the reasons why the Dutch government started to implement strong policies supporting hydrogen and renewables, is the high dependency on fossil fuels, the necessity to reduce CO_2 emissions. Coal and gas are the main sources for electricity production [6], making the Netherlands a country with one of the largest intensities of carbon dioxide emissions in Europe [7].

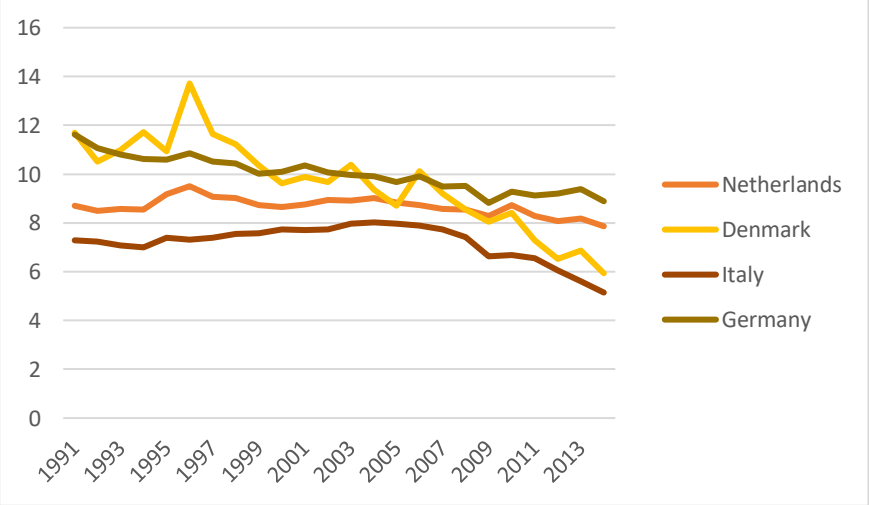

Figure 3 Tonnes of CO2 per capita (t/capita) from fossil fuels burning and from manufacture of cement[1], elaboration of data from World Bank [7].

[1] Carbon dioxide is a by-product of the chemical process that converts limestone ($CaCO_3$) to lime (CaO), in the clinker production, the fundamental component of cement [47]. CO_2 is emitted also in the combustion of fossil fuels to generate the energy to heat up the raw materials to over 1000°C. The overall emissions from cement industry account for about 8% of global CO_2 emissions[48].

The Netherlands have some important natural gas resources, in the northern regions, near Groningen, and offshore, in the North Sea, making the country an exporter of this fuel. According to the BP 2018 review, the total proven gas reserves at the end of 2017 were 0.7 trillion cubic meters, representing 0.3% of global reserves. The ratio between the known reserves, and the yearly production (R/P) is about 17.9, meaning that in less than 20 years the gas reserves of the Netherlands will be over, if the amount of natural gas used per year remains constant. The intense deployment of the reserves of Groningen though, caused severe earthquakes in the region, determining a rising awareness of the public about the urgency of stopping the natural gas production. This has been a strong driver for the Dutch government to start new policies for renewable technology development, and to leave natural gas.

The targets set by Europe in the Climate and Energy package for 2020 have not been met yet, since the Netherlands should reach 14% share of renewables for their gross final energy consumption [8], against the 6% share of 2016 [9].

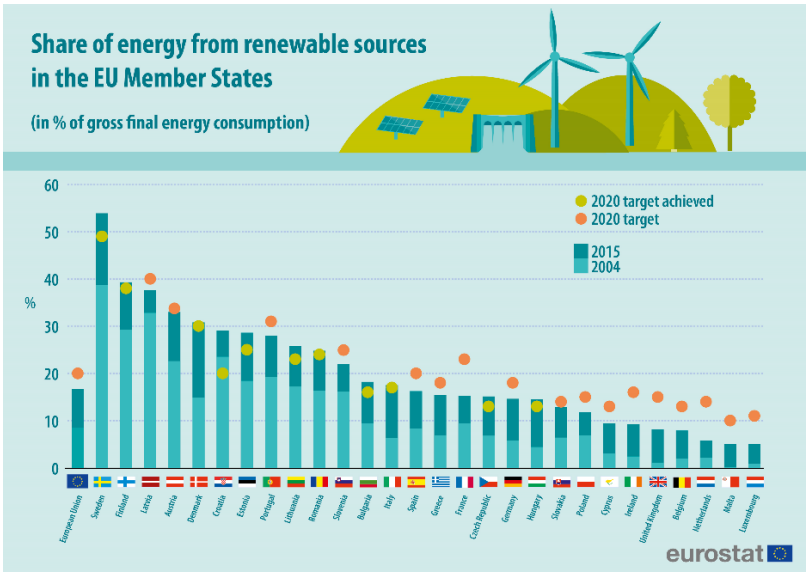

Figure 4 Share of energy from renewables in EU, 2016 [9].

In this framework, the hydrogen initiatives complement the decision of the Dutch government to phase out buildings' connection to the natural gas network within 2050 [10]. Since 2017, new houses are not allowed to use gas for heating and cooking purposes, and the 7 million existing houses will be gradually disconnected from the grid, at the pace of 170,000 dwellings per year. The gas boilers will be substituted mainly by heat pumps system, under the condition of improving the house insulation to reduce the heating demand. To make the CO_2 reduction effective though, the increased electricity demand has to be met by renewables, empowering the "green" energy.

The government is also planning to introduce a carbon floor price, so a tax on the tons of emitted CO_2 [11] for energy producers. The only country that introduced a Carbon Price Floor in the European area is the UK in 2013, which since then saw a significant reduction of electricity produced by coal-fired power plants, considered the main responsible for CO_2 emissions in the energy field. This measure flanked the European Union Emission Trading System, the major carbon market established in 2005 where 31 countries receive or buy carbon allowances that they can trade among each other. The EU established a "cap", which is a target of maximum CO_2 that can be emitted, and assigns the allowances to each country's utilities, who must cover all their emissions to avoid severe fines. The number of credits that can be bought from other companies in Europe and from projects around the world is limited, so that they have a value [12]. When CPF was introduced in the UK, it was supposed to rise every year until 2020 to a value of 30£/tCO_2, but in 2014 the value was set to a threshold of 18£/tCO_2 up to 2021, in order to limit the damage to competitiveness of industries, and to reduce the energy bills for consumers [13]. The law in the Netherlands foresees a growth of the CPF to 43€ by 2030, which is more or less the value that is supposed to have today the carbon according to economists to meet the Paris Agreement goals [14]. The Dutch utilities and industries are opposing to this law, sustaining that it would produce an increase in the import from close countries having a higher emissions intensity, making the reduction of carbon dioxide not effective. Other countries are though planning to phase-out from coal too, and some important utilities like the French EDF, the German E. ON and Denmark Ørsted asked to Europe to introduce a Carbon Price Floor to "speed up the transition to a low-carbon economy" [15]. The objective is to increase the pace of energy transition, making the investments on carbon-free solution more interesting for businesses. There will be a period of subsidies up to 2024, for co-firing coal power plants with biomass, that can keep the five remaining plants still economically sustainable, given the exemption of biomass from carbon tax [11]. The decarbonisation of the Dutch energy system is perceived as urgent especially in the Northern part of the country, where the intensive gas extraction of the last decades caused earthquakes, adding interest in switching from natural gas to hydrogen. Moreover, there is going to be a significant future surplus of energy due to Norwegian hydropower, Danish wind farms, and Dutch and German wind offshore plants, that the electricity transport grid may not sustain [16]. Another sector that could benefit from hydrogen production in the Netherlands is the transport sector, especially the German one, where fuel cells electric vehicles are becoming more and more interesting mobility options. The Northern Innovation Board (Noordelijke Innovation Board) found out that by 2025 or 2030 at maximum, the progress in production, infrastructure, markets and society must be

accomplished to develop the Green Hydrogen Economy [16]. The largest benefit would come from the production of hydrogen from electrolysis (1000 MW) and from the biomass gasification (1000 MW), in combination with the "retrofitting of natural gas pipelines", so the adaptation of the existing infrastructure to ensure the transportation to chemical industries that already use hydrogen for methanol and ammonia production. The overall green hydrogen production coming from the implementation of the previous actions, together with the installation of 4000 MW offshore wind capacity and 100 solar-hydrogen smart areas would bring to the production of 270 000 tH_2. The grid balancing would require only 20 000 tH_2, while most of the market would be in the chemical field, and for export through pipelines.

1.2 Italy

Even Italian governments started to recognize the importance of hydrogen for the sustainable development of the country. The national legislation adapted to the international one, coding the directives for the realization of hydrogen distribution point for vehicles at 700 bar, instead of the 350 bar allowed until now, in the Decreto 23 ottobre 2018 "Regola tecnica di prevenzione incendi per la progettazione, costruzione ed esercizio degli impianti di distribuzione di idrogeno per autotrazione" [17]. The first distribution point for cars and public transport is in Bolzano, but probably a further station will be opened in Milan in 2019, and further projects will be realized. The MISE (Ministero Italiano dello Sviluppo Economico) signed in September 2018 the European Hydrogen Initiative, a non-binding document, stating the political intentions and commitment of the parties to invest in hydrogen, to exploit its flexibility in the energy, transport and industrial fields [18]. In the Italian "Piano Nazionale Integrato Energia e Clima" it is noticed as important to stimulate the research in power-to-gas and power-to-hydrogen technologies to allow a long-term storage for renewable intermittent sources of energy. It is also expressed the willing to implement hydrogen trains for the non-electrified railways of the country (like Valle d'Aosta and Sardinia), and to establish a clear legislation for the injection of hydrogen in the existing gas network. In this sense, Snam, the Italian transmission system operator (TSO) of natural gas, in April started the first experimentation about the hydrogen introduction in the national transport network. A mixture of natural gas and hydrogen at 5% volume concentration is feeding two industries in Contursi Terme, in the province of Salerno.

2. Case study

2.1 The Green Village

The Technical University of Delft started an ambitious project, in collaboration with several departments and local institutions, that foresees the realization of the so-called Green Village: a site inside the campus where innovative solutions for sustainable energy provision, water and waste management can be implemented and tested in a real-life environment [19]. The goal is to accelerate the advancement of disrupting solutions, testing technological and economical criticalities, involving all the important partners -scientists and engineers, industries, the public and the government [20]. Several projects have been already set up, and many others are in the developing phase.

Figure 5 The Green Village current plant.

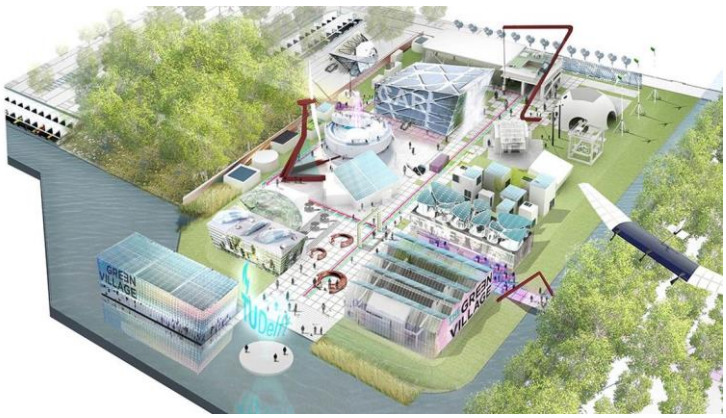

Figure 6 The Green Village future perspective.

There are four fundamental issues that scientists and entrepreneurs working in The Green Village want to address [20]: the clean energy production, the treatment of waste as a resource, the production of clean water, the reduction of pollutants in the air. The place is thought as a space

constantly changing, evolving with the technologies and the systems realized to accomplish the challenging missions aforementioned.

Currently, in The Green Village (TGV) one of the most important concept realized is “Car as a Power Plant”. The project is based on the idea of using the fuel cells vehicles to generate electricity when they are parked, which occurs in 95% of their lifetime.

2.2 Prèt-à-loger house

At the moment, The Green Village heating demand is satisfied through heat pumps, so there is no use of natural gas. The hydrogen is supposed to feed firstly the Prèt-à-Loger house, a student project realized by TU Delft in the context of Solar Decathlon Europe 2014, whose prototype is placed in The Green Village. Its main design idea was to make the implementation of the project replicable for as much dwellings as possible, providing a renovation method for the existing typical Dutch houses (row houses and semi-detached houses where almost 62% of the Dutch population live [21]) without the need of demolition. The architectural element that allows this is the “Skin”: a structure that can be simply added to an already built house, equipped with solar PV panels on the side of the house more exposed to the sun, and with extra-insulation on the opposite side. Moreover, on the sun side, a living space is created to have a buffer zone in terms of temperature, improving the energy performance of the house.

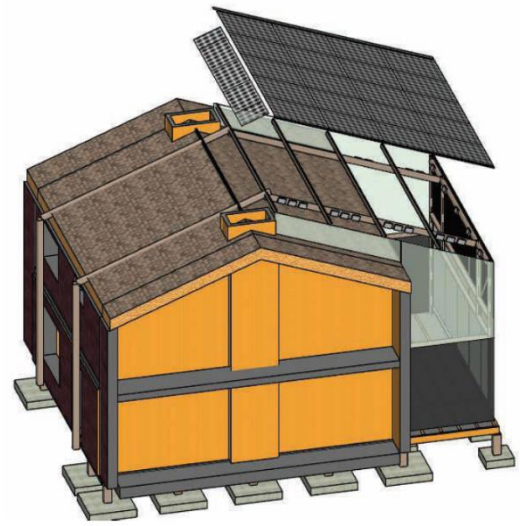

Figure 7 Prèt-à-loger house: the "Skin" pv panels.

Figure 8 Prèt-à-loger prototype.

In conformity with the design concept, the radiators in the house are kept for the heating system, and they are fed by water at low temperature (55°C), which is obtained by the innovative “Solar

Compleet System": a water heater based on heat pumps that use solar panels for the evaporation stage of the refrigerating fluid (R134a). Beyond the absorption of heat from the sun and the environment through thermodynamic black panels, the system is also able to cool down the PV panels on the roof in the hottest days. In winter, it is also possible to use back-up electric heaters that are manually switched on by the house inhabitants, only for space heating. There is one heat pump of 2kW, with a COP that ranges from 3 to 7 according to the outside air temperature, and an identical back-up heat pump for colder winter days [21]. The central heating system (heat pumps) switches on using a thermostat, which can be set manually. The experience has shown that this system is not able to provide the required hot water in some days, which is a further reason of interest for replacing the heat pumps with a hydrogen boiler.

2.3 The H_2 network

In this context, the network companies Stedin, Alliander and Enexis Group built a small hydrogen gas network in The Green Village (TGV), using standards and materials that are commonly employed for natural gas. The objective is to get knowledge and experience in converting the existing natural gas network into a hydrogen network, for those end-users that cannot switch to heat pumps or district heating. Using hydrogen produced from renewable sources can be a valid alternative to reduce CO_2 emissions.

The layout of the gas network has been provided as Autocad file by Stedin. Pipelines have been deposited underground, the first connection will be with the Prèt-à-loger house. The design criteria can be found in the document provided by Stedin "Configureren Dimensioneren gasnet en aansluitinge"[22]. The grid is dimensioned so that is able to regularly feed the dwellings at an outside temperature of -12°C, in contrast with what was made in the past, that consisted in dimensioning on the basis of the peak hour consumption in the coldest day of the year 2014. The gas delivery, must be such that it is at least equal to the expected peak hour consumption, increased of a safety margin of 15%. When the design is made for new buildings, and so the yearly consumption data are not known, it is assumed that the peak hour consumption is 1.1 m^3/h/dwelling in main pipes, while the volumetric hourly consumption in connection pipes must be calculated with some empirical and non-linear formula according to the number of houses that are going to be connected to the grid. The consumption is assumed maximum when the outside temperature is -12°C, and then linearly decreasing as the temperature increases. The line goes close to zero when the outside temperature is 18°C, because it is assumed that at that temperature the end-user will not

switch on the heating system. It is not exactly zero from that temperature up, but assumed equal to 10% of the peak hourly consumption, because of the Domestic Hot Water (DHW) production.

In principle, building this function allows to reconstruct the yearly consumption profile, once that the temperature profile is known.

Gas networks are composed of several elements. There is usually a system of gas transport characterized by high pressure pipelines transporting gas from production areas and regassification stations of Liquified Natural Gas. The location of natural gas reserves is usually many kilometres far from the places where it is consumed. Along the path, pressure drops occur (about 0.1 bar/km [23]), so compression stations are necessary to keep the pressure level high as designed. Then, the gas is either directly delivered to large customers, such as gas-fired power plants and large industries, either delivered to local distribution networks, that carry the natural gas to small customers, like households, commercial customers or public services[23]. The pressure is reduced through several stages in regulation and reduction stations to allow the connection with end-users. The gas can be also stored underground (Underground Gas Storage) during summer, to ensure the security of supply during winter peaks of demand. The same function is led by Line Packing, the storage of gas inside the pipelines obtained increasing the operating pressure up to the maximum allowed by technical and legal constraints.

The Green Village gas network is designed on two main levels of pressure, reported in Tab. 1 together with the different diameters of the corresponding pipelines. It does not have any compression stations, since the hydrogen is supposed to be fed already in pressure and the distances to be covered are short, and there are two reduction stations both reducing the gas pressure from Medium Pressure (MP) to Low Pressure (LP).

Pressure	8 bar_g	100 $mbar_g$
Diameter	50.8 mm, 63 mm	110 mm, 63 mm, 32mm

Table 1 Pressure levels in the Green Village hydrogen network.

There is an external ring at 8 bar_g (MP), and two extraction points in it that lead to two separate reduction stations: “ds”, district station, that is supposed to provide gas to multiple end-users, and “as”, standing for “afleverset” (delivery set), that serves the gas for a single client (the Prèt-à-Loger in this case).

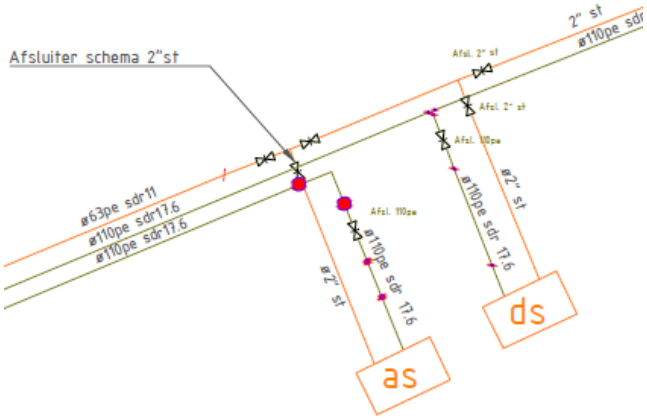

Figure 9 District reduction station ("ds") and Prèt-à-loger reduction station ("as"). Orange line 8 bar_g, green line 0.1 bar_g.

Then a 100-$mbar_g$ ring (Low Pressure, LP) starts from the reduction stations, with a pipeline section of 110 mm. There is a junction point where the pipeline directed to the student houses area starts, and where another pipeline conducts to outlets near the offices and to the Prèt-à-Loger house.

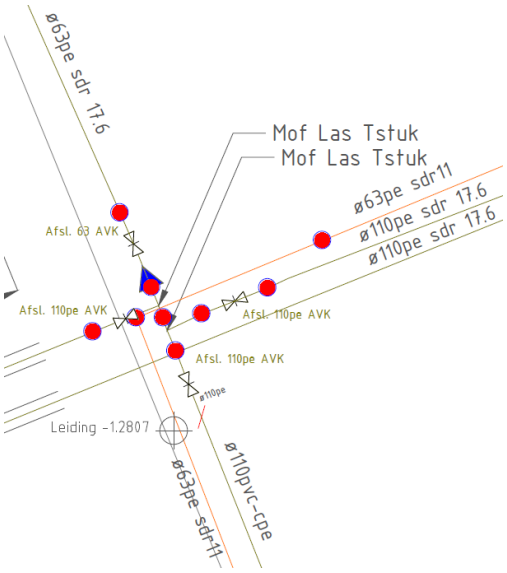

Figure 10 Zoom on crossing of pipelines.

Inside the house, a final reduction of pressure to 30 $mbar_g$ is expected, but this is not considered inside the boundaries of the problem. A schematic of the layout of the network under analysis has been reproduced in fig.11 to show how the nodes where numbered. The lengths, diameters and roughness of pipelines are reported in table 2.

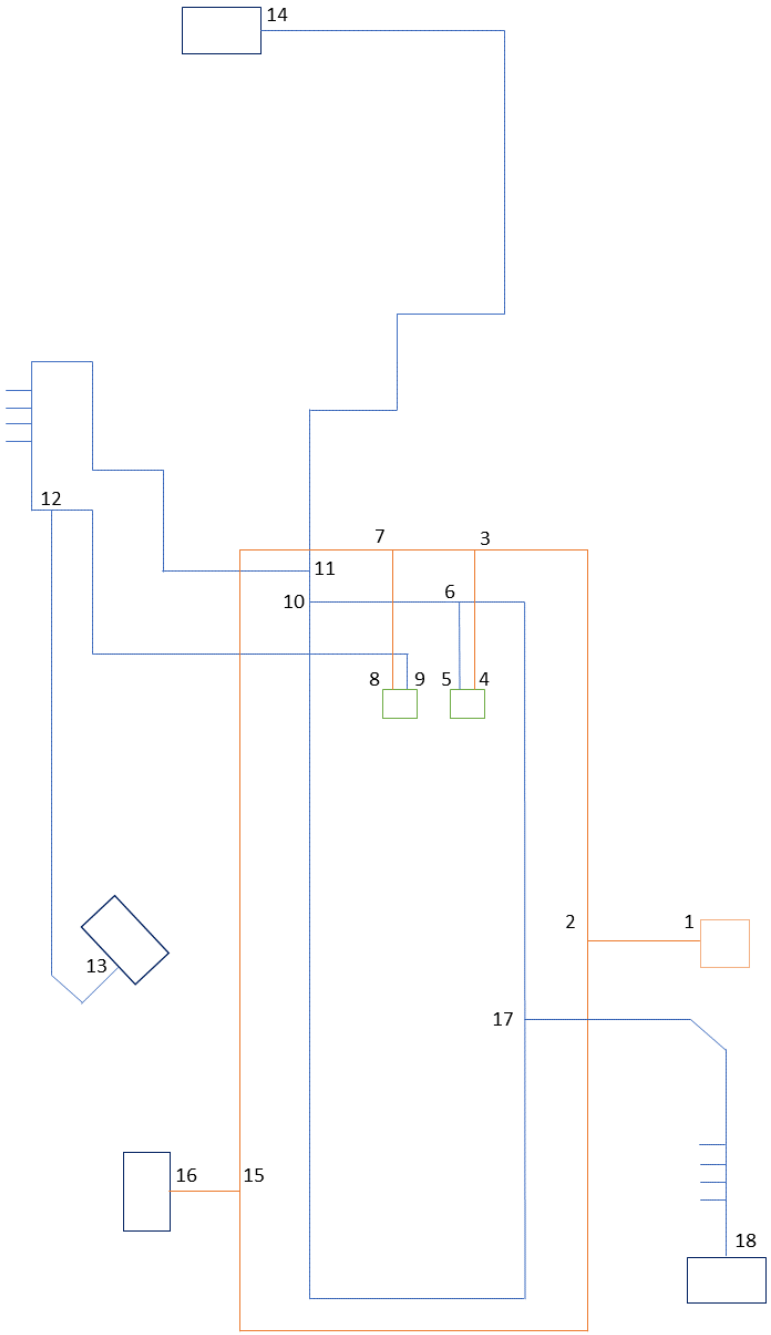

Figure 11 Schematic of the layout

The reduction stations correspond to the branches 12 and 14. The materials constituting the pipelines are: steel (roughness = 45µm [24]), polyethylene (roughness = 3µm[24]), a mixture of polyvinyl chloride and polyethylene postchlorated (pvc-cpe [25], roughness = 1.5µm[24]).

Branch	Entering Node	Exiting Node	D [m]	L [m]	Epsilon [µm]
1	1	2	0.051	13.6	45
2	2	3	0.051	29.2	45
3	3	4	0.051	3.1	45
4	5	6	0.110	2.8	3
5	6	10	0.110	20.1	3
6	7	8	0.051	3.3	45
7	9	12	0.110	36.3	3
8	12	11	0.110	28.6	3
9	11	14	0.063	97.4	3
10	10	17	0.110	90.1	1.5
11	12	13	0.032	47.5	3
12	4	5	0	0	0
13	3	7	0.051	2.6	45
14	8	9	0	0	0
15	7	15	0.063	53.5	3
16	15	16	0.063	12.9	3
17	15	2	0.063	56.2	3
18	17	18	0.110	34.9	3
19	17	6	0.110	29.5	1.5
20	10	11	0.110	2.7	1.5

Table 2 Branches' lengths, diameters, and pipe roughness.

The layout has been simplified to get a clearer vision of the connections.

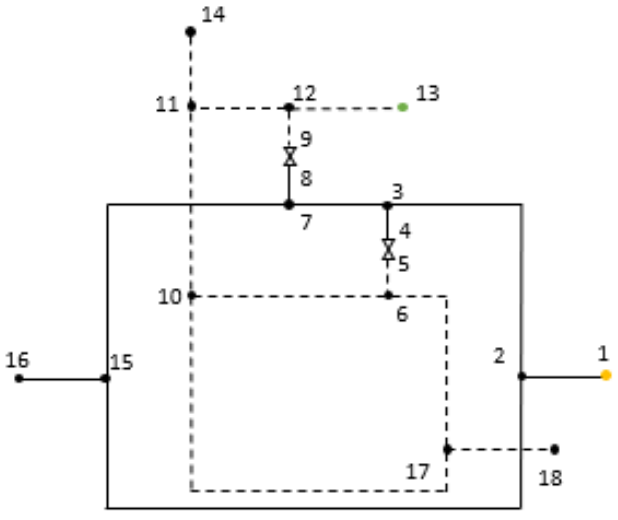

Figure 12 Simplified network layout.

The solid line corresponds to the medium pressure pipelines, while the dashed line is the low pressure one. The node 1 is the inlet for hydrogen tanks, while 16 is the node of the carport, chosen as the potential node for electrolysers, because of its proximity to PV production sites. Node 13 is the Prèt-à-loger, while node 14 is for future connections of the network to the student houses in the area.

3. The gas network transient model

In this thesis, a mathematical model developed in Matlab has been used to simulate the hydrogen behaviour inside the pipelines. The gas models can be substantially divided in two groups, steady-state models and transient models. The first ones are more suitable for designing and optimization processes, while the second ones, which use more complicated equations, are able to simulate pressure changes and line packing evolution, so they are more useful for the dynamic analysis of systems.

The fluid-dynamic problem is described by a set of equations that are intrinsically non-linear and dependent from the solution, therefore some simplifications must be sometimes adopted.

A gas flowing in a pipeline is subjected to pressure reductions, due to friction, and to temperature variations. In the first place, temperature variations are due to heat exchange with the soil, whose temperature can be considered constant during the year. Moreover, because of the Joule-Thompson effect, the gas can reach temperatures slightly lower than the soil during decompression, and sometimes the friction heating effect can cause a non-negligible temperature increase [26]. Therefore, an isothermal hypothesis neglecting all these aspects can compromise the accuracy of the results, especially when dealing with high pressure.

It is possible to model gas networks using either an isothermal approach, or a non-isothermal approach. If the transients in the network due to the demand are very slow, it is reasonable to assume that the gas has enough time to exchange heat with the surroundings that have a constant temperature, so the gas reaches the thermal equilibrium with it. In the same way, when rapid transients occur, if the change of pressure is considered instantaneous, it is possible to consider the process adiabatic, as if the gas has no time to exchange heat with the soil. M. Chaczykowski and A. J. Osiadacz [27] showed that sometimes these assumptions are not good to well estimate the gas pressure drops along pipelines. In fact, the non-isothermal model produces a larger gas pressure drops along the pipeline with respect to the isothermal one. This is because the decrease of density translates in less mass that can be transported at a certain velocity, resulting in a smaller pressure at the end of the pipeline considered. The study sustains the importance of cooling the gas, not only to avoid damage to transmission pipelines, but also to improve the efficiency of the whole compression process.

M. Chaczykowski and A. J. Osiadacz made also a comparative study of one-dimensional, steady-state gas flow models, in non-isothermal conditions, to predict temperature and pressure drops profiles along horizontal natural gas pipelines [28]. The importance of predicting correctly the temperature gradient is evident when the goal is to minimize the temperature dependant terms of the compressor power, while pressure drop calculations are useful both for design and operation of complex networks. Mass balance, energy and momentum conservation laws are used in the numerical approach, in two cases: first, implementing the complete equations, and second, neglecting the convective term of the momentum equation and the kinetic contribution in the energy equation. Then, temperature and pressure drop profiles are obtained using the analytical approach, like in the model used for this study, through ideal gas equation and real gas equation. Then, the outputs of the two approaches are put in relation with some field data collected in Poland, on a line having also a compression station, and working at 55-65 bar_g. As far as the pressure profile is concerned, both numerical and analytical approach showed an optimal correspondence with field data. The most inaccurate results of temperature are instead given by the analytical method that uses ideal gas approximation. This means that first, the simplification made in the momentum and energy conservation laws is not affecting the quality of the output of the model; second, it shows that the real gas equation is fundamental to have valid predictions of temperature by the model when using analytical approach.

In this study, the phenomena determining a temperature variation are neglected, so that the gas properties can be considered constant and the problem is simplified.

The model used is suitable for transient operation, so it provides the simulation of the response of the system when the consumption is changing in time, to get a better representation of the reality. It is based on the paper written by Pambour and others "An integrated transient model for simulating the operation of natural gas transport system"[23]. The model has been developed for transport system but used for the small distribution system in The Green Village.

The network is represented with "edges", standing for pipelines, compression stations and reduction stations, and "vertices", which are the inlet/outlet points and the junctions between edges. The network is described from a topological point of view, through nodes, branches and loops.

The hydraulic behaviour of a gas in a pipeline can be described by the equations of thermodynamics and fluid dynamics, namely the conservation of mass, the conservation of momentum (Newton's second law of motion), the conservation of energy (first law of thermodynamics) and the real gas

law. Considering a general pipeline and applying the previous equations to an infinitesimal control volume (CV) of constant cross-section A and infinitesimal length dx and assuming the parameters averaged along the section A, it is possible to write a set of three Partial Differential Equations (PDEs), and the equation of state.

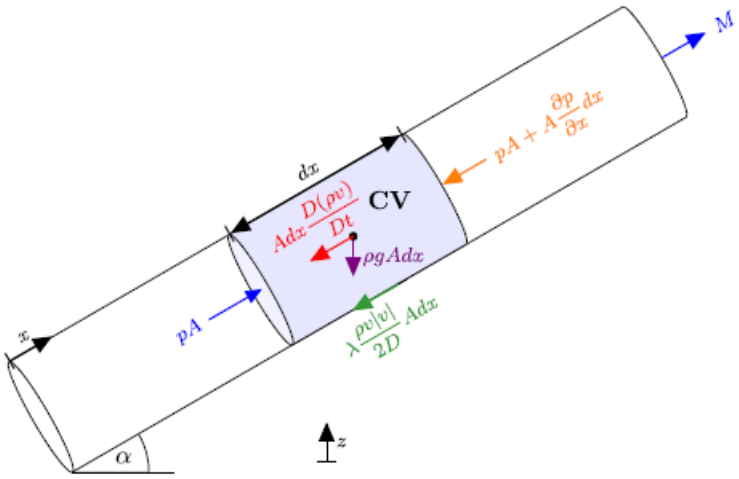

Figure 13 Forces acting on a control volume in a general gas pipeline [24].

Conservation of mass – continuity equation:

$$\frac{\partial \rho}{\partial t} + \frac{\partial (\rho v)}{\partial x} = 0 \tag{1}$$

Conservation of momentum – Newton's second law of motion:

$$\frac{\partial (\rho v)}{\partial t} + \frac{\partial (\rho v^2)}{\partial x} + \frac{\partial p}{\partial x} + \frac{\lambda \rho v |v|}{2D} + \rho g \sin \alpha = 0 \tag{2}$$

Inertia + Convective term + Pressure force + Shear force + Force of gravity = 0

Conservation of energy – first law of thermodynamics:

$$\frac{\partial}{\partial t}\left[\left(c_v T + \frac{1}{2}v^2\right)\rho A\right] + \frac{\partial}{\partial x}\left[\left(c_v T + \frac{p}{\rho} + \frac{1}{2}v^2\right)\rho v A\right] + \rho v A g \sin \alpha = \dot{\Omega} \tag{3}$$

Real gas equation:

$$\frac{p}{\rho} = zR^*T \tag{4}$$

In which z is the compressibility factor and its calculation depend on the method adopted, p is the pressure (Pa), ρ the density (kg/m^3), R^* the elasticity constant ($\frac{J}{kg\ K}$) and T the temperature (K). The choice of the method to be used is very important when dealing with pure methane or natural gas mixtures, as stated in literature. It is more difficult to find reference for network models using pure hydrogen.

The choice of the equation of state in a non-isothermal transient natural gas flow model is not affecting at all the pressure and flowrate time evolution, as found out in [29]. The equations of state used are the AGA-8, SGERG-88, BWR (Benedict-Webb-Rubin) and SRK (Soave-Redlich-Kwong), which are the most frequently used in the gas and petroleum industry. The temperature time evolution figure shows slightly smaller values when AGA and SGERG methods are implemented for the calculation of the compressibility factor, so the compressor power calculated using the results of the simulation would be slightly smaller. A study to compare the results of several equations of state is conducted and shown in paragraph 3.4 of this thesis, with the isothermal hypothesis.

The shear force term in the momentum equation (2) is derived from the Darcy-Weisbach relation, which links the frictional shear stress τ with the dynamic pressure $\frac{\rho v^2}{2}$ through the friction factor λ:

$$\tau = \lambda \frac{dx}{D} \frac{\rho v|v|}{2}$$

For turbulent flow the friction factor λ is generally determined by the Coolebrook-White correlation, which is though implicit in λ, so to avoid the iterative solution an explicit approximation is chosen, the one by HOFER, which uses the pipeline roughness r and the Reynolds number:

$$\lambda = \left[2\log_{10}\left(\frac{4.518}{Re}\log_{10}\left(\frac{Re}{7}\right) + \frac{r}{3.71D}\right)\right]^{-2}$$

With Re defined through gas density ρ, gas velocity v, pipeline diameter D and kinematic viscosity η, as:

$$Re = \frac{\rho v D}{\eta}$$

3.1 Simplifying assumptions

In systems with a large number of connections and elements the problem-solving process becomes highly expensive in terms of computational costs and memory, so some assumptions are considered in the reference paper [23] to make the problem easier to be solved, maintaining at the same time an acceptable level of accuracy.

Firstly, the flow is considered isothermal. In fact, the gas temperature evolution is due to the Joule-Thompson effect, that describes the temperature variation occurring after a compression or decompression, and to the heat exchange with the surrounding soil. To properly represent the phenomena, it would be necessary to know the ground thermal resistance and temperature space distribution, which are both difficult to estimate. Moreover, the flow is usually enough slow ($v < 15\ m/s$) to allow the heat exchange between the gas and the soil, which can be considered in thermal equilibrium. In the light of these considerations, it is reasonable to consider the temperature constant in time and space. This implies that the energy equation (3) is redundant and that it is possible to write the following relation involving the speed of sound c:

$$c^2 = zRT = \frac{p}{\rho}$$

Secondly, the previous consideration about the relatively slow gas flow leads to the assumption of creeping motion. This can be verified comparing the orders of magnitude of the convective and the pressure terms in eq. (2), since they both are derivatives with respect to the space coordinate x, for typical gas pipelines velocity ($v = 10\ m/s$) and the speed of sound ($c = 300\ m/s$):

$$\frac{\partial(\rho v^2)}{\partial x} + \frac{\partial p}{\partial x} = \frac{\partial}{\partial x}\left[p\left(\frac{v^2}{c^2} + 1\right)\right] =$$

$$\frac{\partial}{\partial x}\left[p\left(\frac{10^2}{300^2} + 1\right)\right] = \frac{\partial}{\partial x}[\,p\,(10^{-3} + 1)] \approx \frac{\partial p}{\partial x}$$

This evaluation shows that the convective term is negligible compared to the pressure term when the gas flows in pipelines. The momentum equation can be furtherly developed using the definition of mass flow rate M, as product of density at normal conditions ρ_n and volume flow rate Q:

$$M = \rho_n Q = \rho v A$$

The momentum equation becomes then:

$$\frac{\partial\left(\frac{Q\rho_n}{A}\right)}{\partial t}+\frac{\partial p}{\partial x}+\frac{\lambda(\frac{Q\rho_n}{A})\left|\frac{Q}{A}\right|}{2D}+\left(\frac{p}{c^2}\right)g\sin\alpha=0$$

$$\frac{\partial p}{\partial x}=-\frac{\partial\left(\frac{Q\rho_n}{A}\right)}{\partial t}-\frac{\lambda\left(\frac{Q\rho_n}{A}\right)\left|\frac{Q}{A}\right|\left(\frac{\rho_n c^2}{p}\right)}{2D}-\left(\frac{p}{c^2}\right)g\sin\alpha$$

$$\frac{\partial p}{\partial x}=-\frac{\partial\left(\frac{Q\rho_n}{A}\right)}{\partial t}-\frac{\lambda\rho_n^2c^2}{2DA^2p\eta_e^2}Q|Q|-\left(\frac{p}{c^2}\right)g\sin\alpha$$

The factor η_e is the efficiency introduced to account for the curvature of pipelines in the definition of the effective friction factor λ_e:

$$\sqrt{\frac{1}{\lambda_e}}=\eta_e\sqrt{\frac{1}{\lambda}}$$

The final expression of the momentum equation is then:

$$\frac{\partial p}{\partial x}=-\frac{\rho_n}{A}\frac{\partial Q}{\partial t}-\frac{\lambda\rho_n^2c^2}{2DA^2p\eta_e^2}Q|Q|-\frac{g\sin\alpha}{c^2}p \tag{5}$$

The equation means that the pressure changes along the space coordinate are due to the gas inertia, to the gas flow frictional resistance, which are both opposite to the gas flow acceleration, and to the gravity, according to the inclination of the pipe. It assumes the name of Fast Transient Equation (FTE).

The continuity equation (1) can also be written in terms of pressure variation during time as function of volume flow rate Q:

$$\frac{\partial\left(\frac{p}{c^2}\right)}{\partial t}+\frac{\partial\left(\frac{Q\rho_n}{A}\right)}{\partial x}=0$$

$$\frac{\partial p}{\partial t}=-\frac{c^2\rho_n}{A}\frac{\partial Q}{\partial t}$$

In transient conditions, there is an imbalance between incoming and outgoing flow at the boundaries of the pipeline segment considered, because of the storage of gas in the pipeline itself, that

determines pressure variation in time. At steady-state, the balance is established, and the flowrate is constant ($\frac{\partial Q}{\partial t} = 0$).

A third assumption can be made in some cases. If the load demand is not rapidly changing in time, it is reasonable to neglect the inertia contribution. The momentum equation becomes then:

$$\frac{dp}{dx} + \frac{g \sin \alpha}{c^2} p = - \frac{\lambda \rho_n^2 c^2}{2DA^2 p \eta_e^2} Q|Q| \tag{6}$$

Which is also called Slow Transient Equation.

In the specific case of the small distribution network at The Green Village, it is not possible to make this last assumption, since the gas demand changes frequently in time, so it is necessary to implement the eq. (5).

3.2 Solution implementation

The FTE is a partial differential equation of the first order, whose solution is implemented introducing an implicit time integration in $\Delta t = t_{n+1} - t_n$.

The pressure p is substituted with the square pressure $P = p^2$, so the FTE can be rewritten as:

$$\frac{\partial P}{\partial x} + \frac{g \sin \alpha}{c^2} P = - \frac{\rho_n}{A} \frac{\partial Q}{\partial t} p - \frac{\lambda \rho_n^2 c^2}{2DA^2 \eta_e^2} Q|Q|$$

The equation is then written as finite difference equation, including the time discretization:

$$\frac{dP^{n+1}}{dx} + \frac{2g \sin \alpha}{c^2} P^{n+1} = - \frac{2\rho_n p^{n+1}}{\Delta t A} (Q^{n+1} - Q^n) - \frac{\lambda \rho_n^2 c^2}{DA^2 \eta_e^2} Q^{n+1}|Q^{n+1}|$$

Using averaged properties over the pipe segment $\Delta x = l$ on the right-hand side, it is possible to write the formula for corrected pressure drop collecting the constant properties in the coefficients R_i and R_f:

$$\Delta P^{n+1} = R_f |Q^{n+1}| Q^{n+1} + R_i (Q^{n+1} - Q^n) \tag{7}$$

In which

$$\Delta P^{n+1} = P_1^{n+1} - P_2^{n+1} e^s, \qquad s = \frac{2g(H_2 - H_1)}{c^2}, \qquad R_f = \frac{16 \lambda \rho_n^2 c^2 l_e}{\pi^2 \eta_e^2 D^5},$$

$$l_e = \begin{cases} l, & H_1 = H_2 \\ \frac{e^s - 1}{s} l, & H_1 \neq H_2 \end{cases} \qquad R_i = \frac{2\rho_n L_e p_m}{\Delta t A}, \qquad p_m = \frac{2}{3}\frac{(p_1^2 + p_1 p_2 + p_2^2)}{p_1 + p_2}$$

The corrected square pressure drop ΔP, with e Euler's number, depends on the volume flowrate Q in a non-linear way, through the pipe resistance R_f and the inertia expressed by R_i. Because of the non-linearity of the expression, it is necessary to first linearize the equation and then solve for each time step and for each pipeline. Basically, the pressure drop curve is approximated with a tangent line in a specific point of the curve. Considering a pipe defined in its boundaries by i, j, around a point k, the linearization is conducted as follows:

$$\Delta P_{i,j}^{k+1,n+1} - \Delta P_{i,j}^{k,n+1} = \left.\frac{d\Delta P_{i,j}^{k,n+1}}{dQ_{i,j}^{k,n+1}}\right|^k \left(Q_{i,j}^{k+1,n+1} - Q_{i,j}^{k,n+1}\right)$$

The pressure drop derivative centred in the point k, at timestep $n+1$ for the pipeline i, j is:

$$\left.\frac{d\Delta P_{i,j}^{k,n+1}}{dQ_{i,j}^{k,n+1}}\right|^k = 2R_f + \left|Q_{i,j}^{k,n+1}\right| + R_i$$

Substituting:

$$\Delta P_{i,j}^{k+1,n+1} = \Delta P_{i,j}^{k,n+1} + \left(2R_f \left|Q_{i,j}{}^{k,n+1}\right| + R_i\right)\left(Q_{i,j}^{k+1,n+1} - Q_{i,j}^{k,n+1}\right)$$

Developing the equation:

$$\Delta P_{i,j}^{k+1,n+1} = \Delta P_{i,j}^{k,n+1} + \left(2R_f \left|Q_{i,j}^{k,n+1}\right| + R_i\right)Q_{i,j}^{k+1,n+1} - \left(2R_f \left|Q_{i,j}^{k,n+1}\right| + R_i\right)Q_{i,j}^{k,n+1}$$

$$\Delta P_{i,j}^{k+1,n+1} - \left(2R_f \left|Q_{i,j}^{k,n+1}\right| + R_i\right)Q_{i,j}^{k+1,n+1} = \Delta P_{i,j}^{k,n+1} - \left(2R_f \left|Q_{i,j}^{k,n+1}\right| + R_i\right)Q_{i,j}^{k,n+1}$$

Then $\Delta P_{ij}^{k,n+1}$ is written according to equation (7) and substituted, so some terms cancel among each other, and the final form comes out:

$$\Delta P_{i,j}^{k+1,n+1} - \left(2R_f \left|Q_{i,j}^{k,n+1}\right| + R_i\right)Q_{i,j}^{k+1,n+1} = -R_f \left|Q_{i,j}^{k,n+1}\right| Q_{i,j}^{k,n+1} - R_i Q_{i,j}^{k,n} \qquad (8)$$

The square pressure drop ΔP can be converted to normal pressure drop Δp simply dividing the pressure drop equation by $\left(p_i + p_j e^{\frac{s}{2}}\right)$. Every pipeline is divided in several sections along their length, every section is a control volume and the quantity of gas exchanged among the sections

depends on the pressure between point i and point j, inertia, on the flow resistance and on the gravity force according to the expression (2).

The gas network system is represented through the graph theory, as stated in the previous paragraph, by nodes and edges. The nodes are the interconnection points between elements, and they can be of different kind: demand, where gas is extracted, supply, the entry points of gas flow, storage, where gas can either enter or exit like in the underground gas storage, and junction. The directed edges are elements with an inlet and an outlet for the flow. Compressors, regulators and valves, are considered active elements, because their operation can be controlled by external commands. On the other side, pipelines and resistors (meters, coolers, heaters, scrubbers, etc.) are passive edges, because their behaviour can be fully described by physical equations. The overall topology of the network is synthetized through a node-branch incidence matrix A, whose dimension is given by the product of n number of nodes by m number of branches, with $a_{i,j}$ elements of the matrix:

$$A = [a_{i,j}]^{n \times m}$$

$$a_{i,j} = \begin{cases} +1, node\ i\ is\ outlet\ of\ element\ j \\ -1, node\ i\ is\ inlet\ of\ element\ j \\ 0, node\ i\ and\ element\ j\ disconnected \end{cases}$$

Moreover, it is useful to split the matrix A in pipe (A_P) and non-pipe (A_N) elements. Each node is characterized by a nodal pressure and a nodal load L_i, and each branch by a volume flowrate, such that the load is positive if it is a demand node (negative for supply nodes), while the flowrate is positive if the flow direction is from inlet to outlet (negative instead).

The conservation of mass equation (1) is written in finite difference form as well, so that it can be implemented in a software environment. The relation shows that the nodal pressure may change if there is an imbalance between inflow and outflow of a certain nodal volume. The corresponding form is:

$$\frac{V_i}{\rho_n c_{i,j}^2} \frac{dp_i}{dt} = \sum_{j=1}^{k} a_{i,j} Q_{i,j} - L_i \tag{9}$$

This equation is written for every node, and then an implicit time integration is performed, for a time step of $\Delta t = t_{n+1} - t_n$. The resulting matrix equation is:

$$\Phi p^{n+1} - A_P Q^{n+1} - A_N Q^{n+1} + L^{n+1} = \Phi p^n \tag{10}$$

Where $\Phi = diag\{\Phi_1, \Phi_2, \dots, \Phi_n\}$, $\Phi_i = \frac{V_i}{\rho_n c_{i,j}^2 \Delta t}$, $V_i = \frac{\pi}{8} \sum_{j=1}^{k} D_{i,j}^2 \Delta x_{i,j}$

This finite difference matrix equation needs additional relations in order to close the problem, because of the great number of unknowns. For this purpose, beyond the momentum equation (2), it's necessary to write some linear equations describing the control mode of non-pipe elements, like compressors and regulators, and the control of entry and exit nodes, of demand, supply and storage.

The generic equation for non-pipe element j, with inlet node i and outlet node $k \neq i$ is the following:

$$C_{p,j,i} p_i^{n+1} + C_{p,j,k} p_k^{n+1} + C_{Q,j} Q_j^{n+1} = E_j$$

Where $C_{p,j,i}$, $C_{p,j,k}$, and $C_{Q,j}$ are scalar coefficients of inlet node, outlet node and flowrate in element j, respectively. E_j is a constant. Compressors and regulators may have constraints of operation, like the minimum and maximum pressure allowed, or flowrate, that will be checked during the time integration.

The equation for i-th node control is instead the following:

$$K_{p,i} p_i^{n+1} + K_{L,i} L_i^{n+1} = S_i$$

Where $K_{p,i}$ and $K_{L,i}$ are scalar coefficients for pressure and load, respectively, and S_i the scalar value assumed as set-point in the node by pressure or load. Either the pressure or the load has to be known for the future time step t_{n+1}, accordingly to the nature of the node control. Even for these nodes there are some constraints on maximum and minimum load or pressure, which will be checked in the transient simulation.

Collecting all the equations in a matrix form the following set of equations is obtained:

$$\begin{pmatrix} \Phi & -A_P & -A_N & I \\ A_{DP} & -R & 0 & 0 \\ C_P & 0 & C_N & 0 \\ K_P & 0 & 0 & K_L \end{pmatrix} \begin{pmatrix} p^{n+1} \\ Q_P^{n+1} \\ Q_N^{n+1} \\ L^{n+1} \end{pmatrix} = \begin{pmatrix} \Phi \mathrm{p}^{\mathrm{n}} \\ B \\ E \\ S \end{pmatrix} \tag{11}$$

The first row represents the set of continuity equations, distinguishing between pipe (pedix P) and non-pipe (pedix N) elements, the second row is instead the momentum equation, with A_{DP} pipe-node incidence matrix, R diagonal matrix representing the slope of the linearized pipe equation, and B the intersection with the y-axis. Finally, the third and fourth rows are the control equations for non-pipe elements and for node facilities, respectively.

The algorithm starts with the estimation of the steady-state solution, representing the initial condition. The network is then discretized in space (Δx) and time (Δt), and the results of the steady state are assigned to each node and branch of the network, so that pipe flows and nodal pressures are defined before the time loop. The transient simulation starts, first with an approximation of the linearized pressure drop, and then with the solution of the matrix above (11). The matrix resolution is repeated iteratively for k steps until the norm of the residual vector becomes smaller than a set tolerance (usually smaller or equal to 10^{-3}). The residual vector is calculated using the pressure and flowrate values resulting from the transient calculation:

$$Res = \Delta P^{n+1} - \left[R_f |Q^{n+1}| Q^{n+1} + R_i (Q^{n+1} - Q^n)\right]$$

Usually the converged solution is obtained within 1-5 iterations. The procedure is repeated for the time duration established for the analysis, checking at every time step that the constraints of non-pipe elements and facility nodes are satisfied.

The small network analysed in this work does not require the implementation of equations to describe the control operation of compressors or resistors, which are not present, nor the equations for valves, since the ones in the network are maintenance and safety valves (operational modes not considered in this study). The only non-pipe elements would be the reduction stations that adjust the pressure from 9 bar to 1.1 bar, for the district distribution (not planned to be working in the immediate future) and for the Prèt-à-loger house. To reduce the numerical problems coming from the implementation of the reduction stations in the model, the two pressure lines are treated separately, split in two: the inlet of the reduction station is considered as an outlet node of the medium pressure network with constant exiting flowrate, while the reduction station outlet is considered as the feeding point of the low-pressure line, at constant pressure.

The model is tested over several network configurations:

1. Base case: the medium pressure network has one inlet and one outlet, as well as the low pressure one. The first stage of experimentation in The Green Village will have this configuration.

2. PàL case with electrolysers: the medium pressure network has two inlets, one for hydrogen tanks and the other for electrolyser, and one outlet. The low-pressure network still has just one inlet and one outlet.

3. District case: with respect to the previous case, there is one more outlet directed to further end-users.

The objective is to show the pressure drops and flowrate trends. The model is also able to show the line-packing capacity, so the storage capability of the pipelines that can be useful during peak hours or for buffer storage.

3.3 Comparison of equations of state in isothermal conditions

The Equation of State is the analytical expression relating the pressure to the temperature and the volume [30]. The simplest one is the expression obtained with the ideal gas approximation, that is based on two assumptions:

- the volume of the gas molecules is negligible if compared to the total volume and the distance between the molecules;
- there are no attractive or repulsive forces between the molecules.

The equation found is:

$$p = \frac{RT}{v} \tag{12}$$

In which "R" is the universal gas constant (8.314 J/(mol K)), "v" is the molar volume (m^3/mol), "T" is the temperature (K) and "p" the pressure (Pa).

This equation is applicable for values of pressure and temperature close to the ambient conditions, while to represent the behaviour of real gases in extended ranges of pressure and temperature, other relations had to be developed.

Although the maximum pressure of the hydrogen gas network in TGV is not very high (8 bar_g), a comparison among different equations of state is conducted to understand how they differ from the ideal gas equation. The equations implemented for the comparison are the Van der Waals, the Noble-Abel and the Leachman's NIST, beyond the ideal gas one. The objective is to represent the

density as function of pressure, at fixed temperature. The baric range chosen goes from 0.1 bar_g to 8 bar_g, and the temperature chosen is 10°C, the plausible soil temperature in winter.

Firstly, Van der Waals in 1873 tried to eliminate the assumptions of the ideal gas model to represent the real behaviour of gases. At high pressure, the volume occupied by molecules must be considered, so he introduced the co-volume *b* to subtract from the effective molar volume *V*. In order to account for the molecular attraction, he developed the parameter *a*, that is considered as a measure of intermolecular attraction. The ideal gas equation modified by Van der Waals is:

$$p(T, v) = \frac{RT}{v - b} - \frac{a}{v^2}$$

The value of the parameters *a* and *b* depend on the critical point of the substance, and they are taken from the paper [31]:

$$a = 0.0247 \frac{J * m^3}{mol^2}$$

$$b = 2.65 \cdot 10^{-5} \frac{m^3}{mol}$$

The ideal gas equation (12) can also be expressed in the cubic form, in terms of volume *V*:

$$v^3 - \left(b + \frac{RT}{p}\right) v^2 + \left(\frac{a}{p}\right) v - \left(\frac{ab}{p}\right) = 0$$

It has three possible values of *v*, and one at least is real. This form has been implemented in Matlab, to solve the polynomial equation for several interesting values of pressure. Among the three solutions found, only one is real, and it is converted into density dividing the molar weight [kg/mol] by the molar volume [m^3/mol].

Although the Van der Waals equation provided a more realistic explanation of the gas behaviour, it was still not suitable for design purposes in the hydrocarbon industry, that pushed the research further. A known simplified version of the Van der Waals equation is the Noble-Abel equation:

$$p(T, v) = \frac{RT}{v - b} \tag{13}$$

Rewriting for the density:

$$\rho = \frac{MM}{\frac{RT}{p} + b} \tag{14}$$

Where *MM* is the molar mass of hydrogen, b is the co-volume, R is the universal gas constant. This formulation does not take into account the intermolecular forces, so it is applicable for gas at high temperature, when kinetic energy of particles is so high that the attraction between them can be neglected.

The last implemented equation of state is the Leachman's formulation developed in 2009 for the National Institute for Standards and Technology (NIST) in Boulder, Colorado [32]. The modern equations of state are explicit in terms of reduced Helmholtz free energy α, as function of reduced temperature and density:

$$\frac{a(T,\rho)}{RT} = \alpha(\tau,\delta) \tag{15}$$

$$\tau = \frac{T_c}{T}$$

$$\delta = \frac{\rho}{\rho_c}$$

In which $a(T,\rho)$ is the Helmholtz free energy depending on temperature and density, T_c and ρ_c are the critical temperature and the critical density, respectively.

The reduced Helmholtz free energy is composed of two parts, the ideal-gas contribution α^0 and the residual contribution α^r:

$$\alpha(\tau,\delta) = \alpha^0(\tau,\delta) + \alpha^r(\tau,\delta) \tag{16}$$

Both terms are obtained through non-linear regression techniques, from literature and experimental data.

The reduced ideal-gas Helmholtz free energy, already reformulated in a computationally convenient expression, is:

$$\alpha^0 = \ln\delta + 1.5\ln\tau + a_1 + a_2\tau + \sum_{k=3}^{N} a_k \ln[1 - \exp(b_k\tau)] \tag{17}$$

a_k and b_k can be found in the tables inside the NIST paper [32].

The residual contribution to the reduced Helmholtz free energy is:

$$\alpha^r(\tau,\delta) = \sum_{i=1}^{l} N_i \delta^{d_i} \tau^{t_i} + \sum_{i=l+1}^{m} N_i \delta^{d_i} \tau^{t_i} \exp(-\delta^{p_i}) + \sum_{i=m+1}^{n} N_i \delta^{d_i} \tau^{t_i} \exp[\varphi_i (\delta - D_i)^2 + \beta_i (\tau - \gamma_i)^2] \tag{18}$$

Values of $N_i, d_i, t_i, p_i, \varphi_i, \beta_i, \gamma_i$, and D_i are collected in tables inside the paper, whilst $l = 7, m = 9$, and $n = 14$.

The NIST equation can be applied for ortho-hydrogen, para-hydrogen, and normal hydrogen. The difference between the first two is the spin state. Heisenberg called "ortho", the hydrogen that dominates at room temperature, and "para" the other one which becomes prevalent at low temperature. Normal hydrogen is a mixture of both, in the ratio 3:1 respectively, and corresponds to the composition of the hydrogen at room temperature. The properties of this last type are chosen for the calculations.

The thermodynamic properties can be calculated through the relations suggested in [32]. In fact, the relation used in the Matlab code for the comparison is:

$$p(T,\rho) = \rho R T \left[1 + \delta \left(\frac{\partial \alpha^r}{\partial \delta}\right)_\tau\right] \tag{19}$$

Since it has not been possible to find a relation where the density is a function of the pressure, the opposite approach has been used with respect to the other EOS: scanning different values of density, the derivative of the reduced residual Helmholtz free energy is calculated, and the pressure is obtained as a consequence of the equation (19).

The derivative with respect to δ of the residual Helmholtz free energy has been manually computed, considering τ constant. The results of the comparison are shown next.

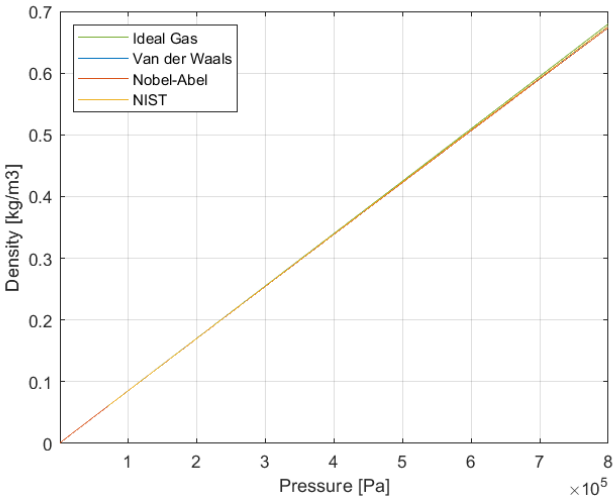

Figure 14 Density vs pressure for different equations of state.

It comes out that in the range of pressure of interest for the operation of the network there is no major difference in the choice of the equation in terms of resulting density. The deviation from the ideal behaviour is more evident as the pressure increase, since the molecular volume becomes less and less negligible, as well as the attraction between molecules.

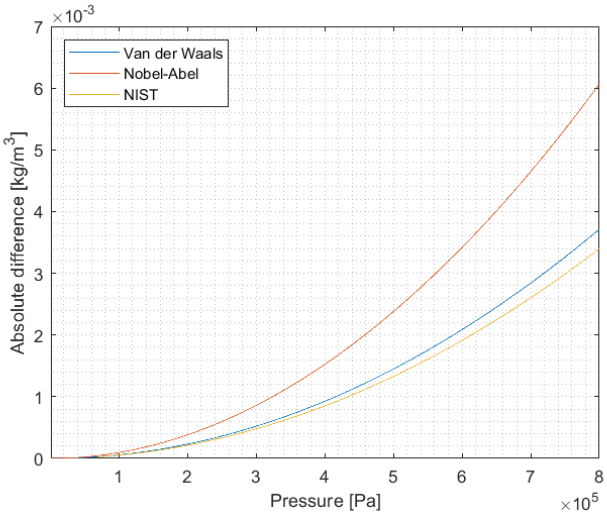

Figure 15 Absolute difference with respect to ideal gas equation vs pressure.

The difference is calculated with respect to the density obtained with the ideal gas approximation. The density values obtained with the Noble-Abel equation, are the furthest both from the ideal gas density values, and the V.d.W and NIST values. First, the co-volume is considered, which makes the density smaller with respect to the ideal case. Second, the neglection of the attraction term results in a smaller density than the one obtained without this assumption.

The Van der Waals equation has been implemented in the Matlab model, because it represents a good trade-off between simplicity and accuracy.

4. Data profiling

4.1 Consumption data

The model requires gas consumption data with a high time resolution. In the Green Village, the heat pumps electric consumption has been loaded on the data collection platform in the past years, but it has never been checked. It turned out that the profiles are not representative of any physical behaviour, resulting constant all over the year (Appendix). Since the real data cannot be used in this case, it is necessary to model the consumption.

The method used by Stedin to foresee the gas consumption during the design phase consists in supposing a linearly decreasing trend of consumption with outside temperature increase. This procedure allows to get a rough estimation of the gas profile, as a function of outside air temperature [22].

The outside temperature is measured in a site 1 km far from TU Delft Campus, with a frequency of measurement of 1 minute, by a PhD student of Process & Energy department. The original set of data is the following:

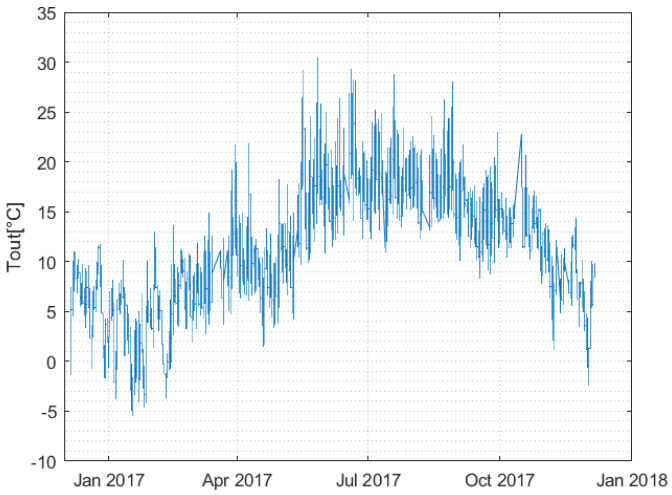

Figure 16 Temperature evolution data measured over 2017.

The temperature data are averaged on an hourly basis for January, the coldest month, and shown below:

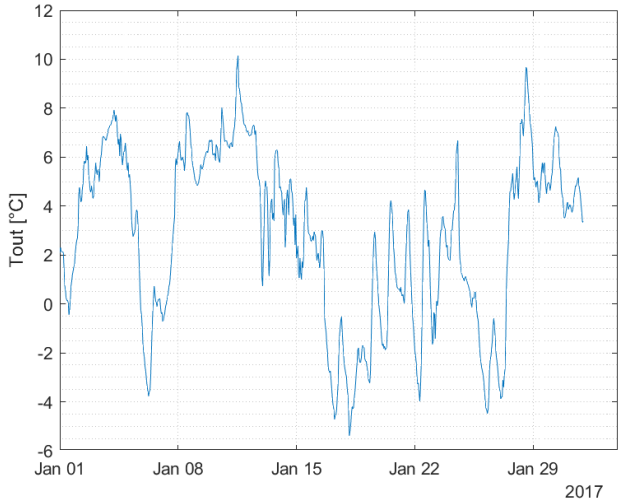

Figure 17 Hourly average of the temperature data set.

Then, the linear function used by the company to simulate the gas flowrate consumption is easily reconstructed, considering a peak hourly load of 1.1 Nm^3/h/dwelling when the outside temperature is -12°C, and a consumption at 18°C that is 10% of the maximum consumption, so 0.11 Nm^3/h/dwelling:

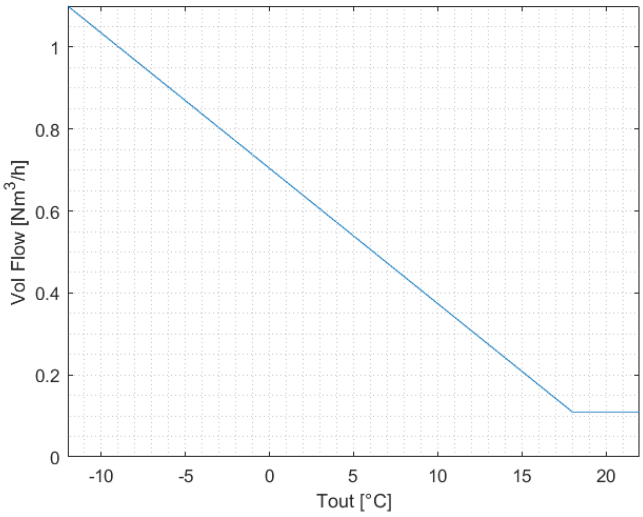

Figure 18 Volumetric consumption function of outside temperature, from Stedin.

$$VolFlow\ [\frac{Nm^3}{h}] = \begin{cases} -0.033 \cdot T_{out} + 0.704 & -12 \leq T_{out} \leq 18 \\ 0.11 & T_{out} > 18 \end{cases}$$

The expected hourly average volumetric consumption in the month of January is obtained using the previous function, and then converted into power demand (kW) through the lower heating value of natural gas, considered constant and equal to 9.31 kWh/Nm^3 [32]. Multiplying the two values, the heating demand is obtained:

$$Q_{h,T}\ [kW]\ = VolFlow\left[\frac{Nm^3}{h}\right] \cdot LHV\ \left[\frac{kWh}{Nm^3}\right]$$

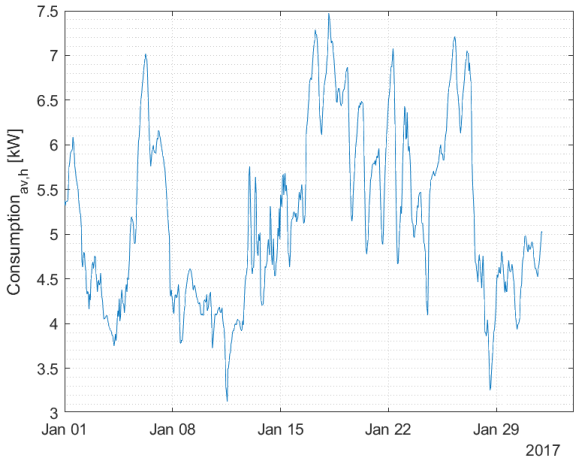

Figure 19 Average hourly consumption in January 2017 using temperature function.

The lowest temperature in the year 2017 was registered the 18th of January, with an average hourly temperature of about -5.4°C, corresponding to the maximum demand of about 7.5 kW.

The profile derived from the outside ambient temperature does not consider the fact that during the night, when the temperature is the lowest and consumption is expected to be the highest, the heating system usually switches off. Moreover, the function does not account for the consumer behaviour, which is more likely to need the hot water in the morning, and during meals, when he/she is at home.

A similar, but more refined technique is explained in the 2017 paper [33]: the Standard Load Profiles (SLPs) generated at Technical University of Munich (TUM) in 2002, updated during the years, are used by more than 83% of the gas network operators (2014). They have been derived by measurements conducted by the gas utility companies on customers in order to get forecast for future energy demand. Nevertheless, the SLPs based on historical data are not helpful to make long-term forecasts, because they do not take into account the improvements in building insulations, and the more efficient heating systems. The temperature dependent load profile that TUM derived is a combination of a sigmoid term, whose coefficients are extracted from historical profiles, and a linear

term, that is composed of a line for space heating (subscript H) and a line for water heating (subscript W):

$$h(T) = \left[\frac{A}{1 + \left(\frac{B}{T - T_0}\right)^C} + D\right] + \left[\max\begin{Bmatrix} m_H * T + b_H \\ m_W * T + b_W \end{Bmatrix}\right.$$

The max term is a source of non-linearity which is eliminated re-writing the term as:

$$Linear_n = a(T_n) * WHL(T_n) + b(T_n) * SHL(T_n)$$

The daily gas demand depends on this function, and on two other factors, the customer value (CV) and the weekday factor (F_{wd}):

$$Q_d = CV * h(T) * F_{wd}$$

The customer value is a scaling factor calculated as the sum of historical daily gas demands divided by the sum of the h-values obtained in the same period. The weekday factor should include the behaviours of customers depending on the day of the week.

The Linear Programming optimization is applied to find the combination of values of a and b (see below) that minimize the difference between the annual demand (which has to be known) and the summation of daily demands:

$$Min\ Obj = AnnualDemand - CV * \sum_{n=1}^{365} F_{wd} * (Linear_n + Sigmoid_n)$$

Where $WHL(T_n)$ and $SHL(T_n)$ refer to the values of water and space heating lines at temperature T_n respectively. There are some constraints on these factors that must be verified

In the analysis of energy demand of buildings, it is becoming increasingly important to evaluate precisely the loads of domestic hot water and space heating, beyond the electricity one, considering the trend of decreasing the supply temperatures. In particular, in local low temperature district heating systems, the occupants' behaviour and the thermal properties of the envelope of the building influence significantly the energy demand, beyond the characteristics of the supply system. The aforementioned points are taken into account in the work of A. Kellert, R. Egelkamp and D. Schmidt [34], through the use of a Visual Basic for Applications (VBA) tool that generates randomized profiles of occupancy, which are then implemented in a thermal simulation that produces detailed hourly heating load profiles. In the first step, the "Profile Maker" uses the hypothesis of Markovian

process, in which the probability of an event depends only on the state of the previous event. Probability density functions from literature and standards are used to simulate the presence and the activities of the inhabitants of the house, as well as if it is a weekday or a weekend day. The output of this step is the occupancy profile, as well as examples of electricity profile, domestic hot water and body heat profiles. Then, the results of this first part are included in the model of a building group, created with TRNSYS. The software is needed to determine the room set-point temperature and the heat losses (and gains), according to the physical properties of the envelope. Several age classes and users' classes are examined and compared. The heating load profiles that come out from the simulation show that the Domestic Hot Water heating demand is highly influenced by the number of occupants in the house, while the Space Heating demand is mainly changing according to the age of the building, and so to the insulation: as the building energy class gets better, the DHW share of heating gets higher.

In this work though, the approach used is different. Typically, in order to estimate the heating demand variation at different locations the Heating Degree Days are used [35].They are defined as the sum of the positive differences between the set-point heating temperature and the outside temperature. HDD are a measure of how much the outside temperature has been below a certain base temperature, and for how long, and they are useful to design heating systems. If the HDD and the yearly heating consumption are known, it is possible to get a daily profile of the demand of a house, through the following formula:

$$TOT_{day\,n} = TOT_{year} * \frac{\left(T_{set,aver} - T_{out,aver,day\,n}\right)^{+}}{\left(\sum_{i=1}^{365}\left(T_{set} - T_{out,aver,day,i}\right)^{+}\right)} = Q_{LPG,SH}$$

In which TOT_{year} is the heating energy consumption over a year expressed in kWh, $T_{set,aver}$ is the daily average set-point temperature, $T_{out,aver,day\,n}$ is the daily average outside temperature in the generic day n. This technique is used by the software LoadProfileGenerator (LPG) to calculate the space heating contribution. Similarly, to split the profile obtained in hourly values, the following formula is used:

$$TOT_{hour\,x} = TOT_{day\,n} * \frac{\left(T_{set}(t_{hx}) - T_{out,aver,hour\,x}\right)^{+}}{\left(\sum_{i=1}^{24}\left(T_{set}(t_i) - T_{out,aver,hour,i}\right)^{+}\right)} = Q_{SH}$$

In which $TOT_{day\,n}$ is the energy consumed in the generic day n (kWh), $T_{set}(t_{hx})$ is the set-point temperature at hour x, $T_{out,aver,hour\,x}$ is the hourly average outside temperature at hour x. The set-

point temperature time profile is taken from a report produced by the Energy Research Centre of the Netherlands (ECN), one of the largest institutes in Europe devoted to conducting research for sustainable energy systems, and the research centre RIGO Research en Advies, both working usually as consultant for the government. The report, available on the website of the central government of the Netherlands [36] is the result of a research conducted by surveys to 4800 households in 2012, to get fundamental insights on the energy performance of the Dutch housing stock and on customers' behaviour, in the context of a research started in 1995 by the Dutch Ministry of the Interior and Kingdom Relations [37].The profile chosen is the one for houses with energy label A.

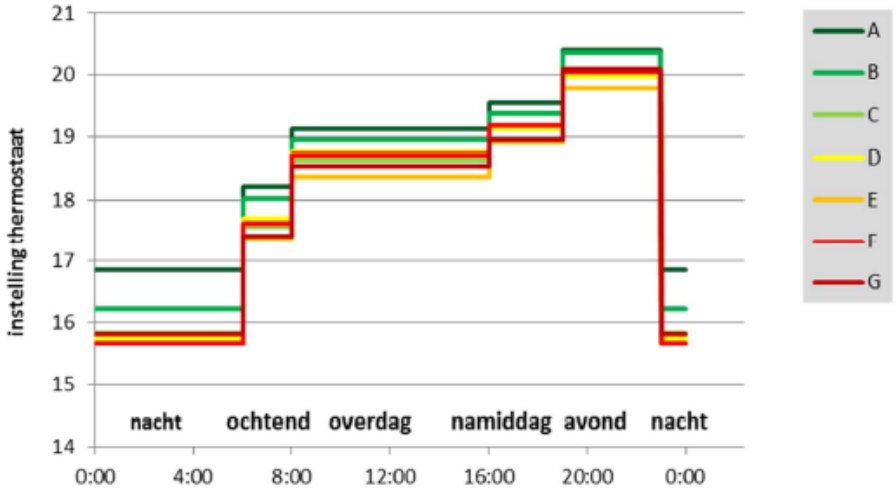

Figure 20 Set-point thermostat temperature in the Netherlands according to the energy label[38].

The A curve is the highest, probably because energy-saving buildings are more insulated, so they have a higher inside temperature for longer time, which allows to set the thermostat to higher temperature. Thanks to the hourly variability of the thermostat set-temperature, it is possible to get a changing daily profile starting from the LPG results on space heating.

The outside temperature hourly dataset used is provided by the KNMI (Koninklijk Nederlands Meteorologisch Instituut), the Royal Netherlands Meteorological Institute, from the closest site to The Green Village. The weather station is the number 344, located close to the Rotterdam airport [38] at about 8 km of distance from TGV. The dataset, comprehending many other information beyond the temperature, is the average of the measurements from January 1991 until February 2019, so it represents an average climatological year for the chosen location. They have an hourly frequency.

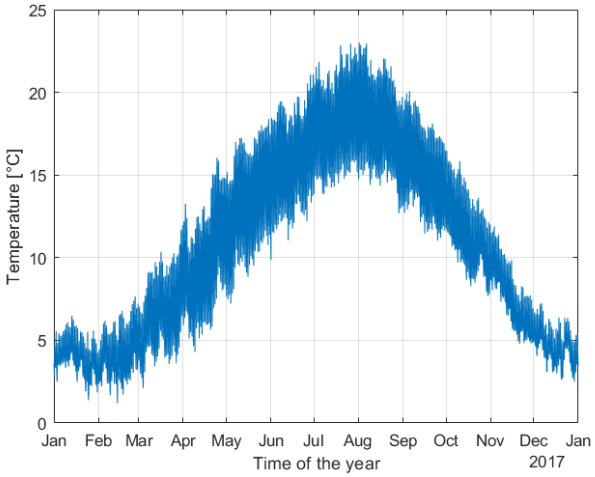

Figure 21 Annual temperature in 2017, KNMI dataset.

In order to have a better understanding of the yearly temperature profile in the selected site, in this work I looked for the most frequent average daily temperatures in each season in which the heating system is supposed to be on. The results of the analysis are summarised below.

	Winter	**Spring**	**Autumn**	**Yearly**
Average [°C]	4.5	11.9	8.9	10.7
Most frequent [°C]	4	9	6	4
Minimum [°C]	3	6	4	3
Maximum [°C]	8	17	15	19

The temperatures in the first row of the table are the result of the mean value of the temperatures of that season. In the Appendix the plots of the frequency of temperatures for the different seasons can be found, while the distribution over the year of the temperature is shown below.

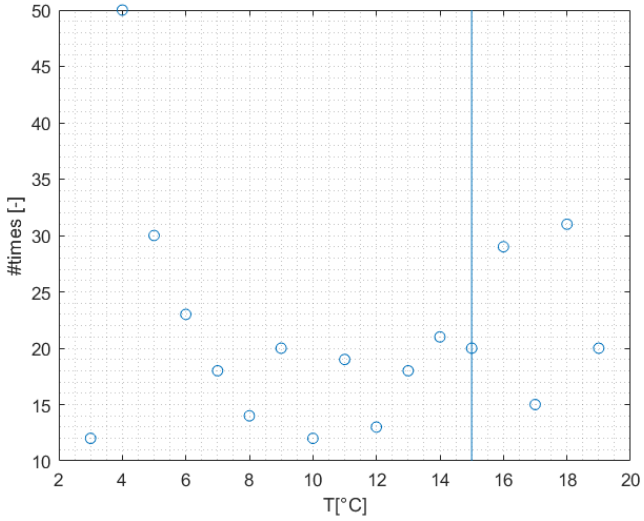

Figure 22 Distribution of daily average temperature during the year 2017. Minimum heating temperature for EU standards is 15°C.

Once that the most frequent temperatures are found, some of the days in which they occur are selected.

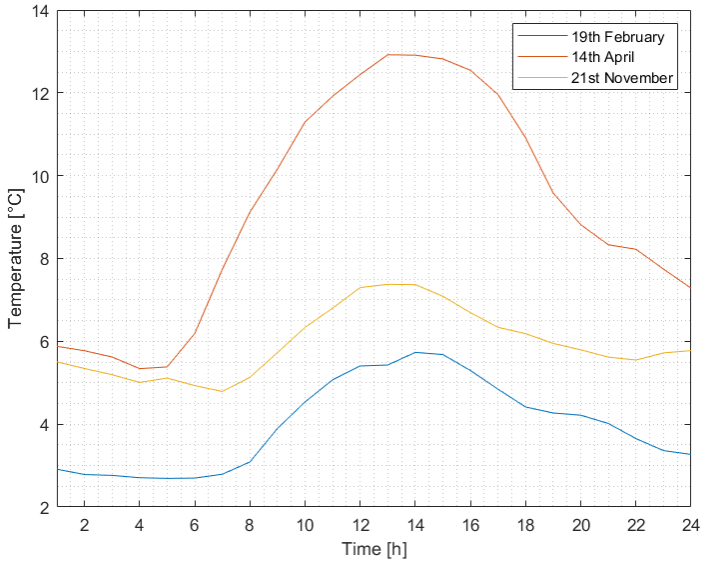

Figure 23 Temperature trend during three representative days of year 2017.

The heating profiles for the same days are coherent with the outside temperature profiles. The heating system is lowered during the night. Below the complete plot of the normalized space heating obtained through the aforementioned method, and the plot focusing on 24h in different seasons are shown.

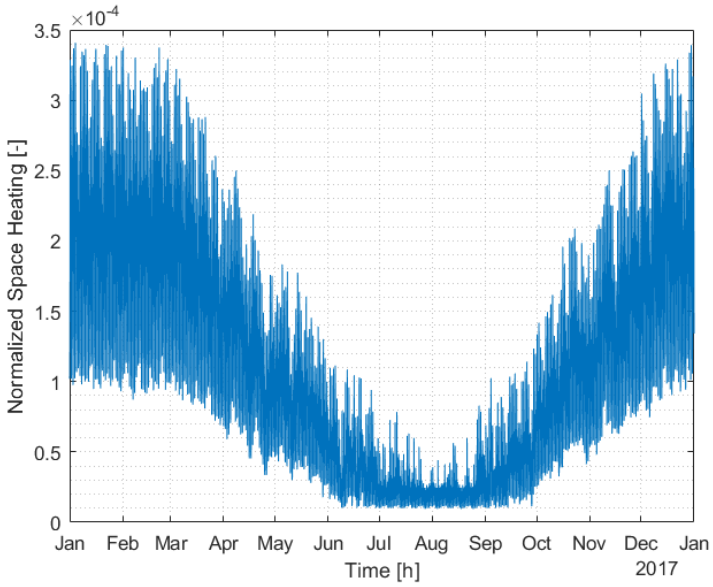

Figure 24 Normalized space heating in 2017 obtained with degree days method.

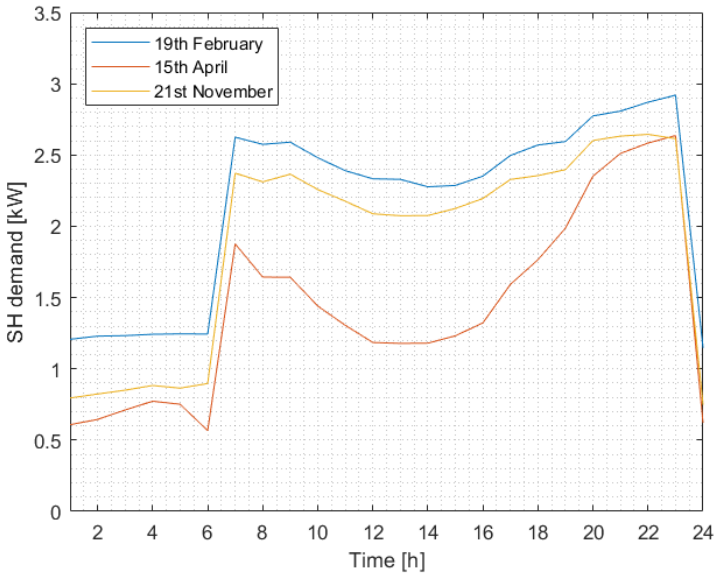

Figure 25 Space heating profiles detail on 24h, for different seasons.

The steep changes occurring at 6:00 and at 23:00 are due to the significant change in the thermostat settings (from 10°C to 18.2°C and from 19°C to 10°C respectively). The plot shows the heating need of the house.

The profiles obtained are compared with the ones available on the website of a Dutch utility company, Liander, which operates in the distribution of electricity and natural gas in some regions of the Netherlands [39]. They collected several measurements from end-users for 20 years until

2007 and created an average normalized set of yearly consumption data, intended to estimate the consumption.

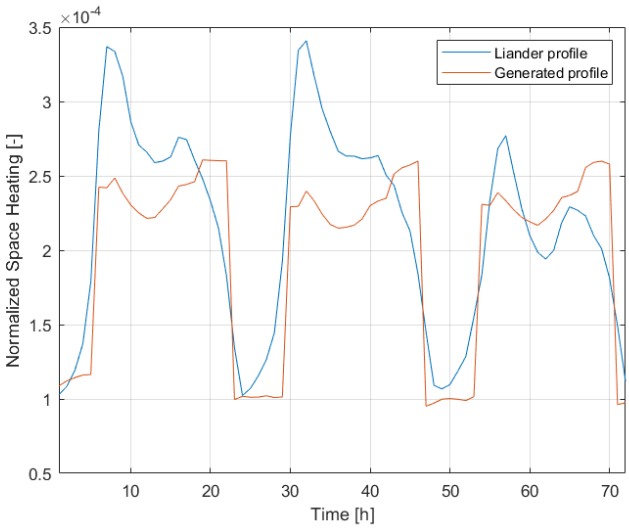

Figure 26 Space heating profile comparison on 19th-20th-21st February 2017.

The profiles are quite similar one another. The peaks of the generated profile are inverted with respect to the ones provided by Liander, coherently with the settings imposed: the higher the set-point temperature of the heating system, the higher the consumption. There is one modification made on the profile found in [37],that consists in reducing the night thermostat temperature from 16.9°C to 10°C, to have a smaller consumption and keep track of the house envelope inertia.

4.2 LoadProfileGenerator software

The hydrogen boiler that is going to be installed in the Prèt-à-loger will produce also the hot water for domestic use, so it is necessary to estimate the energy needed for this purpose as well. The characteristic of this load is that it is highly influenced by the house's inhabitant behaviour, therefore a specific software is used to simulate the household occupancy and activity, LoadProfileGenerator (LPG). It has been developed by Noah Pflugradt for its PhD thesis, in the Technical University of Chemnitz, in 2016. The software creates energy and water load profiles according to the occupancy and behavioural simulation of people in the house, based on the simplified behaviour model from the German psychologist D. Dorner. This model states that every person has certain desires, and he/she will choose the activity that fulfils them, favouring one to another according to the level of satisfaction about that desire in each moment considered [40]. The desires translated into actions, turned into load curves. It allows a detailed modelling of appliances present in the house, and of the occupant profile, to make the simulation as close as possible to reality. In alternative it is possible

to choose among a wide range of possibilities already set in the software. For the simulation, a predefined household has been chosen (male 22-years-old university student), while the appliances present in the Prèt-à-loger have been implemented in the software. It is also possible to specify the location and the temperature profile, that is used in the calculation of the space heating consumption. In fact, LPG implements the Heating Degree Days method: given a total yearly energy consumption for heating to be specified, and an outside temperature time-based profile, it is possible to get a daily profile of space heating. Shown below the electricity and domestic hot water patterns.

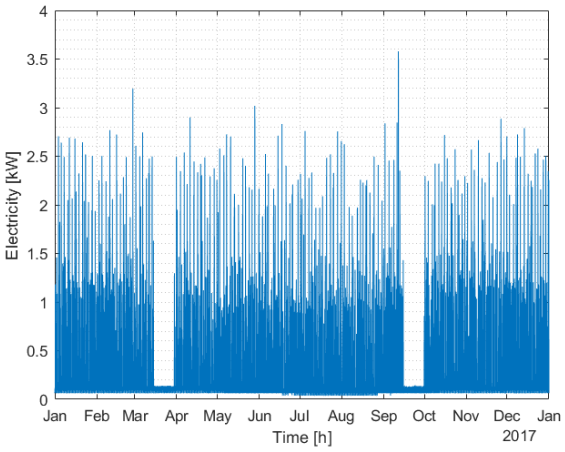

Figure 27 Electricity profile by LPG over the year 2017.

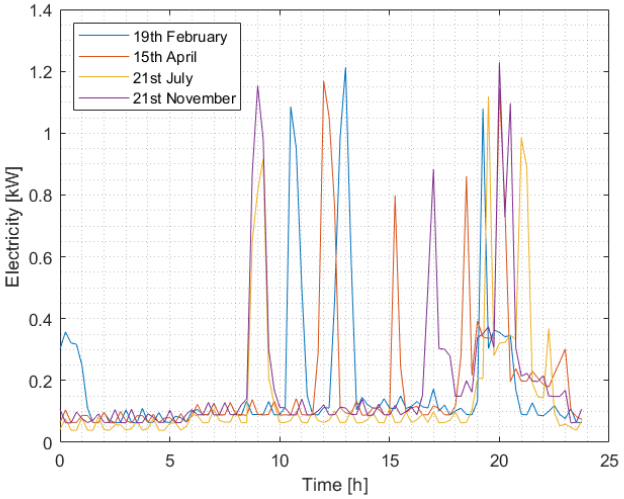

Figure 28 Electricity patterns in four representative days of 2017 by LPG.

The electricity load profile is characterized by a base load more or less constant, probably given by the fridge and the freezer, and some steep demand peaks, whose time occurrence is varying in time, but generally happens twice a day. The software provides a detailed report about the activities made by the house occupant, with a time basis of 1 minute, later aggregated in hourly profiles.

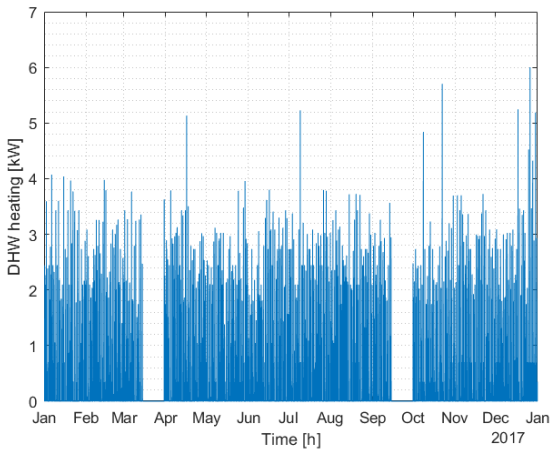

Figure 29 Domestic water heating by LPG in the year 2017.

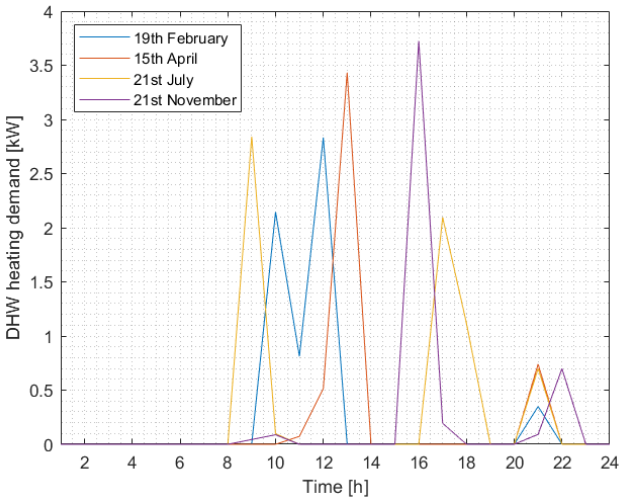

Figure 30 Domestic water heating by LPG in the year 2017.

The domestic hot water profile is even more variable in time, and it presents very high and sudden peaks, that differ a lot among the days considered. The randomness of consumption is well expressed by this non-constant trend.

The heating load of the Prèt-à-loger has been computed considering the natural gas as source of energy. In fact, it has been used as input data the average gas consumption in 2017 in the Netherlands, in the residential sector, as provided by the Dutch research institute for statistics, CBS StatLine [41]. The gas volume value, 1240 Nm^3, has been multiplied by the lower heating value of Groningen Gas, which is about 9.8 kWh/Nm^3 from literature [42], lower than other European supplies.

The profile obtained must be converted into the energy profile corresponding to the hydrogen feeding. This is done considering the efficiency of the natural gas furnace and the one of the hydrogen boiler. Considering Q_{TOT} as the space heating hourly load profile calculated before starting from the LPG profile, η_{ng} as the natural gas efficiency of a common furnace (90%), η_{H_2} as the hydrogen boiler efficiency (87%), the house demand in terms of power to be provided by the hydrogen burner is obtained:

$$Q_{house,SH,H_2} = \frac{\eta_{ng} * Q_{SH}}{\eta_{H_2}}$$

The LPG software simulates the activities, and then it converts them into loads. The warm water for domestic use is calculated in terms of litres consumed every minute, and then converted into an energy load considering the specific heat of water (4.186 kJ/(kg*K)), and a constant temperature difference of 40°C. The multiplications of these three factors produces the profiles shown before. Therefore, the energy that the hydrogen burner needs can be found from the previous profiles divided by the device efficiency:

$$Q_{house,DHW,H_2} = \frac{Q_{LPG,W}}{\eta_{H_2}}$$

4.3 Production data

The scope of this work is to evaluate if it is possible to increase the self-consumption of renewable energy on site producing hydrogen for heating purposes. The photovoltaic production data has been correctly recorded in the Prèt-à-loger, in 2017, both from the carport and from the house, with frequency of a record every 15 minutes.

The PV panels are both on the roof and on the southern façade of PàL, with respectively 35% and 38% transparency factor, to allow the natural lighting to the house during the day. They are part of the "Skin", the integrated system that is conceived to be simply added to an already-built house, whose function is the energy production through photovoltaic panels, and the energy saving acting as a thermal buffer, guaranteeing at the same time a pleasant environment from the aesthetical point of view. The technology used is the mono-crystalline silicon, with an efficiency of about 16.5%. The DC power produced is converted into AC power by an inverter, so in standard test conditions, 21.19A at 230V are obtained. The energy produced is measured by a kWh meter located in the control room of the Prèt-à-loger house, and the data recorded by a pulse sensor fixed on the measuring device [21].

The installed capacity in the PàL is of 4.875 kW_p, occupying a surface of about 35.42 m^2 on the roof (1.77 m^2 per panel, 20 panels installed) and 8.21 m^2 on the windows, for a total surface of 43.63 m^2. The carport has an installed capacity of 4.72kWp, 18 modules for a total surface of 29.42 m^2. PàL and carport PV power production plots are shown below, separately and then in total for the year 2017.

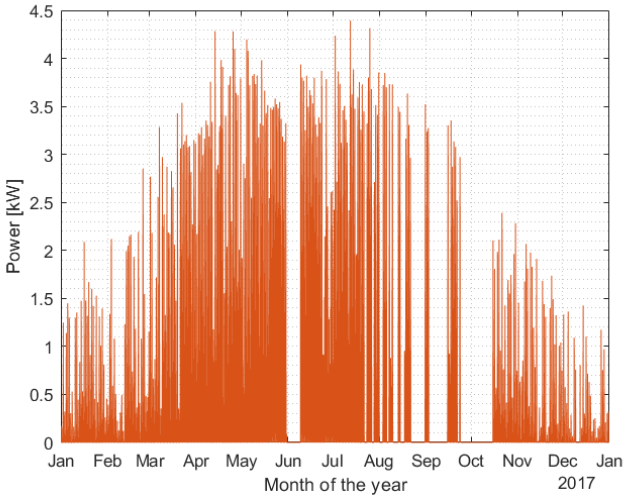

Figure 31 Carport PV production in 2017.

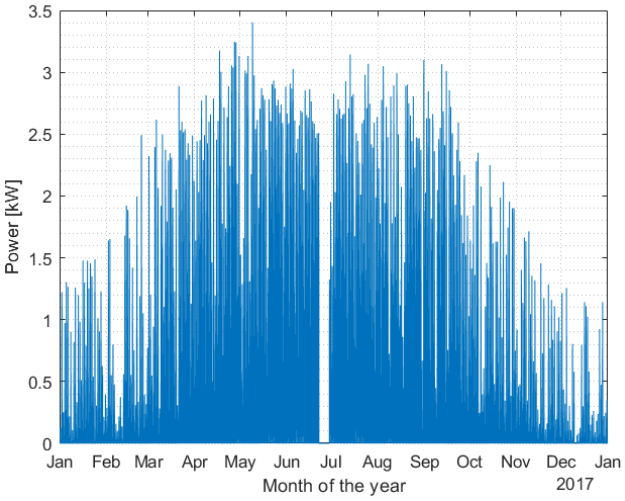

Figure 32 Prèt-à-loger house PV production in 2017.

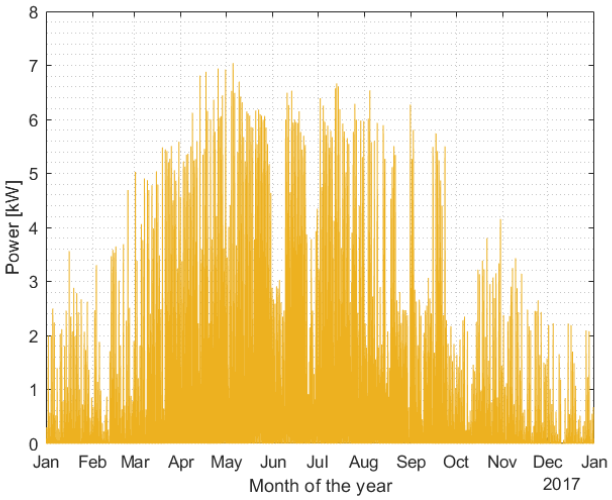

Figure 33 Total PV production in 2017.

4.4 Electrolysis

The hypothetical excess electricity from photovoltaic panels is now sold to the grid, but it represents an opportunity for green hydrogen production by electrolysis of water. The overall water electrolysis reaction is:

$$H_2O \rightarrow H_2 + \frac{1}{2}O_2$$

The device that allows this reaction to take place is an electrochemical system composed of two electrodes, the anode, which is where the oxidation takes place, and the cathode, in which the reduction occurs, and an electrolyte, the ionic conductor. The electrodes are connected to an external electric energy generator producing DC current. Depending on the electrolyte, the reaction occurs under different conditions, and the electrolyser is classified accordingly:

1. Alkaline electrolysis cell (AEC): it works at T<80°C, the electrolyte is an aqueous solution of KOH or NaOH, and the ionic species involved in the reaction are the hydroxyl ions (OH^-);

2. Proton exchange membrane electrolysis cell (PEMEC): it works at T<80°C, the electrolyte is a solid porous polymeric layer, usually Nafion, that allows the proton exchange (H^+ ions);

3. Solid oxides electrolysis cell (SOEC): it works at T>700°C, with a solid electrolyte made normally of yttria-stabilized zirconia, through which the oxygen ions (O^{2-}) flow easily.

To better understand advantages and disadvantages of each system it is interesting to introduce some thermodynamic and kinetic details about electrolysis [43].

The minimum overall electricity that has to be fed from the outside, equivalent to the molar Gibbs free energy $\Delta_r G$, is a composition of the enthalpy of reaction $\Delta_r H$ and the energy associated to the entropy of the reaction at a certain temperature ($T\Delta_r S$). Increasing the thermal energy, so the temperature of operation of the device, produces a reduction of the electricity that must be provided according to the following formula:

$$\Delta_r G = \Delta_r H - T\Delta_r S$$

There are two significant voltages for electrochemical systems, the reversible voltage and the enthalpy voltage. The first one is the open circuit voltage, so the voltage to impose to have the water decomposition, and it is related to the molar Gibbs free energy of formation of water $\Delta_r G$ in kJ/mol, to the number of electrons exchanged (n=2), and to the Faraday constant F=96.485 C/mol:

$$V_{rev} = \frac{\Delta_r G}{nF}$$

The second one, also called thermo-neutral voltage, represents the minimum energy required for the reaction to sustain itself:

$$V_{ent} = \frac{\Delta_r H}{nF}$$

If the voltage provided is smaller than the thermoneutral voltage (but higher than the reversible one), the cell requires heat (endothermic condition), if the voltage is larger than the thermoneutral one the cell releases heat (exothermic condition). So, if the voltage applied to the cell is exactly equal to the thermoneutral one, it operates in adiabaticity. At standard conditions (T=298K and p=1bar) the reversible voltage is 1.23V while the thermoneutral voltage is about 1.48V, meaning that there is a heat demand for the reaction to take place.

Both Gibbs free energy and enthalpy of reaction $\Delta_r H$ depend on temperature and pressure of operation. The voltage must be larger than the reversible voltage to provide for the overpotentials due to oxidation (η_{anode}), to reduction ($\eta_{cathode}$) and to the ohmic resistance of the electrolyte (η_{Ohm}):

$$V_{cell} = V_{rev} + \eta_{anode} + \eta_{cathode} + \eta_{Ohm}$$

The overvoltage terms are calculated by the Tafel relation:

$$\eta_{anode} = \frac{RT}{\alpha_a F}\ln\left(\frac{I}{I_{0,an}}\right) \qquad \eta_{cathode} = \frac{RT}{\alpha_c F}\ln\left(\frac{I}{I_{0,cat}}\right)$$

They represent the activation overvoltage at the electrodes, and they are a function of different terms: I_0 (A) is the exchange current, which is the current measured on the electrodes surface in open circuit conditions, R (J/molK) is the universal gas constant, F (C/mol) is the Faraday constant, T (K) is the temperature and α is the coefficient that expresses the number of electrons exchanged (product of symmetry factor and number of electrons exchanged in the rate determining step). The Ohmic overpotential is defined as function of the electrolyte resistance R (Ω) and the current in the cell I (A):

$$\eta_{Ohm} = RI$$

The most used electrolyser for hydrogen production in the industry is the alkaline one. The cell is composed of two electrodes, anode and cathode, generally made of materials based on nickel, or nickel oxide, and a thin barrier, to separate the products of the reactions occurring at the electrodes. The barrier, called diaphragm, is made of a microporous material, permeable to hydroxyl ions and to water, but able to keep separated the gaseous hydrogen and oxygen produced at the electrodes. Therefore, the main properties must be the high permeation to water, high ionic conductivity, and high resistance to corrosion in strongly alkaline media. Some examples of materials used are poly-ether-sulfones, nickel oxide layers on titanium oxide basis, glass reinforced with polymers [44]. The potassium or sodium weight concentrations in the aqueous electrolyte vary according to the operating temperature between 25%wt to 30%wt for a range of temperatures between 70°C and 100°C and pressures between 1bar and 30bars. During the cell operation, water is reduced at the cathode forming hydrogen and OH^- ions, that flow through the diaphragm to oxidize the water at the anode, according to the following redox reactions:

Anode: $$2OH^-_{(aq)} \rightarrow \frac{1}{2}O_2 + H_2O_{(l)} + 2e^-$$

Cathode: $$2H_2O_{(l)} + 2e^- \rightarrow H_{2(g)} + 2OH^-_{(aq)}$$

Alkaline electrolysis systems employ non-noble electrocatalyst materials, on the contrary of PEMEC that require expensive components (Platinum in the electrodes, Nafion membrane), and they are stable in stationary operation, thanks to lower temperature of operation compared with SOEC, that are subject to cracking after long-term hydrogen production. The diaphragm does not impede completely the gas permeation, that must be checked for safety reasons, since hydrogen is highly flammable.

The alkaline electrolyser cell is chosen for the analysis of integration of renewables with hydrogen production through electrolysis.

From the previous considerations, it is possible to estimate the hydrogen mass flow demand of the Prèt-à-loger house, as well as the mass flow that the photovoltaic energy availability allows to produce. Moreover, introducing the specific consumption of the electrolyser, the electricity demand evaluations can be conducted. The model chosen is the S6 MP of McPhy [45], a specialized company offering a wide range of small capacity alkaline electrolyser for several range of pressures and hydrogen flowrate. The S6 MP can deliver hydrogen up to the pressure of 8 bar_g, and to the maximum flowrate of 4 Nm^3/h. Its specific energy consumption, so the energy needed to produce a unit volume of hydrogen, is 5.25 kWh/Nm^3. This specification allows to calculate the electric power needed to ensure the hydrogen feeding to the house. Before though, it must be calculated the volume flowrate of hydrogen that can be produced, and, by the density [46], the mass flowrate, using the lower heating value of hydrogen 3 kWh/Nm^3 [46]:

$$\dot{m}_{house,H_2} = \frac{Q_{house,H_2}}{LHV_{H_2}} \rho_{H_2}$$

The photovoltaic power production P_{PV} available from measurements in the house is destined to firstly cover the electricity consumption of the house for lighting and appliances, the excess electricity $P_{PV,net}$ is the potential power available for the hydrogen production.

$$\dot{m}_{avail,H_2} = \frac{P_{PV,net}}{SC_{ely}} \rho_{H_2}$$

4.5 Energy mismatch analysis

In order to understand the effective potential of production of hydrogen in the site considered, the power curves are analysed. The photovoltaic power curves are known from measurements, while the consumption curves have been obtained as described in the previous section. The energy produced by the PV panels is used to guarantee the electricity need to the Prèt-à-loger house, then the possible excess can be used in the electrolyser to produce as much hydrogen as possible. The overall energy produced, required for the heating demand and for the electricity is calculated integrating the corresponding power curves over a year.

The available electricity from renewables is shown below:

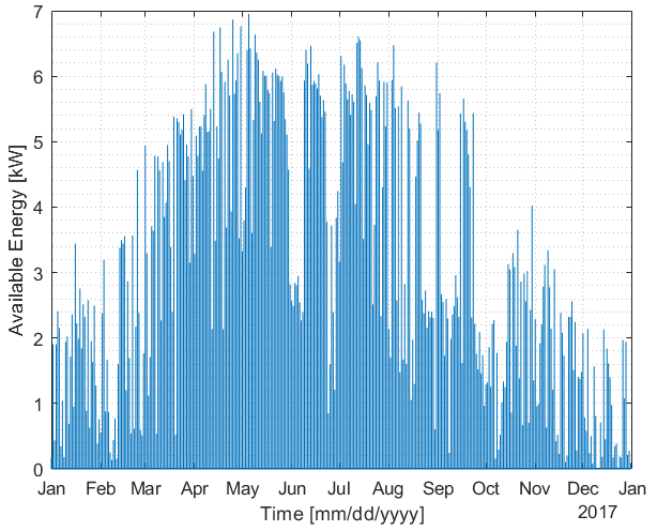

Figure 34 Electricity available, net of self-consumption for appliances and lighting.

It is calculated as the difference between the photovoltaic energy and the electricity consumption, setting zero in the points where the electricity must be taken from the grid because not directly available from the sun.

The electrolyser has a specific energy consumption of 5.25 kWh/Nm^3, that is used in the analysis to determine the electricity needed to produce the hydrogen required for heating. Multiplying this value by the consumption curve the following plots are obtained:

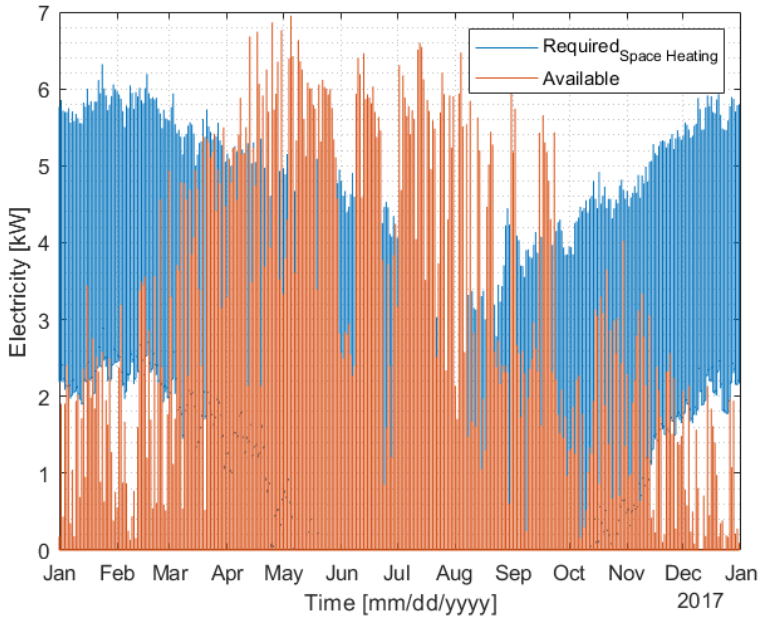

Figure 35 Electricity available, and electricity required by the electrolyser to ensure the space heating need.

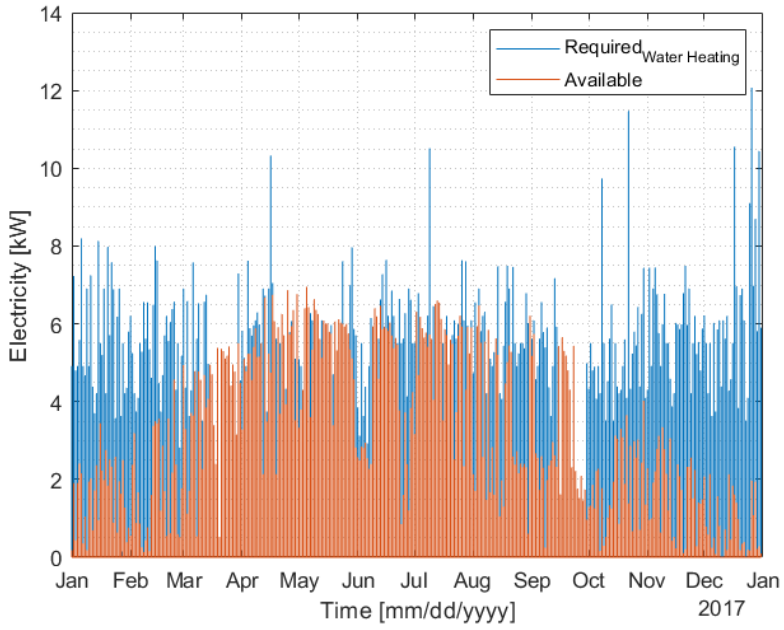

Figure 36 Electricity available, and electricity required by the electrolyser to ensure the domestic water heating need.

The results in terms of energy over the year 2017 are summarized in the table below:

		[kWh$_e$]	[kg]
PV PRODUCTION		**6106**	**104.56**
PàL DEMAND	Lighting, Appliances	1554	-
	Space Heating	21930	375.52
	DHW Heating	2950	50.51

Table 3 Energy production and demand over the year 2017.

The renewable energy available could satisfy the lighting and appliances energy demand, and there would be still 4552 kWh to be used for the hydrogen production. The electricity required for the domestic hot water heating could be provided fully by the photovoltaic.

The time mismatch between the electricity production from renewables and the electricity consumption for heating is not considered in the analysis of the total energy over the year. It is though fundamental to show the actual time production and consumption on the same plot, because renewable energy is intermittent, and non-homogeneous during the seasons. Here below, the mismatch in the significant days already chosen previously is shown, together with the mismatch over each season of year 2017.

	PV PRODUCTION		**PàL DHW DEMAND**		**PàL SH DEMAND**	
	[kWh$_e$]	**[kg]**	**[kWhe]**	**[kg]**	**[kWh$_e$]**	**[kg]**
19th February	4.82	0.082	12.35	0.211	104.18	1.784
14th April	12.78	0.218	10.56	0.180	70.28	1.203
21st July	43.67	0.748	13.77	0.236	9.27	0.159

21st November	0.09	0.001	9.74	0.167	91.41	1.565
Winter	589.67	10.1	703.77	12.05	8023.05	137.4
Spring	2727.31	46.7	830.63	14.22	4825.15	82.62
Summer	1769.22	30.3	821.23	14.06	1419.6	24.3
Autumn	423.27	7.25	797.86	13.66	6646.62	113.82

Table 4 Electricity production and demand for different days and seasons in 2017.

The space heating is too high to be covered by renewables, so in the plots below only the domestic hot water heating demand is considered for the mismatch.

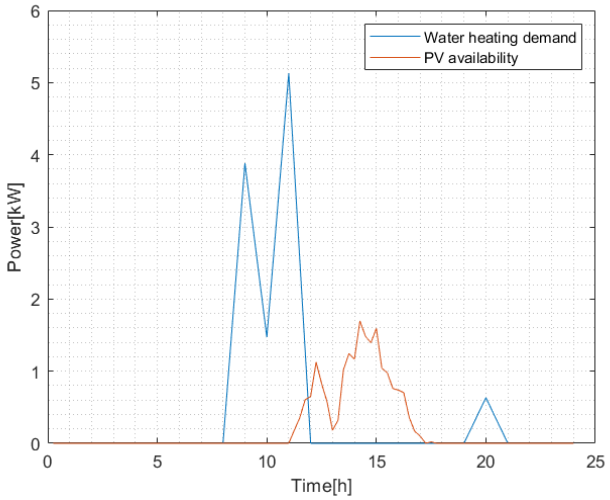

Figure 37 Demand of electricity of the electrolyser for water heating on February 19th.

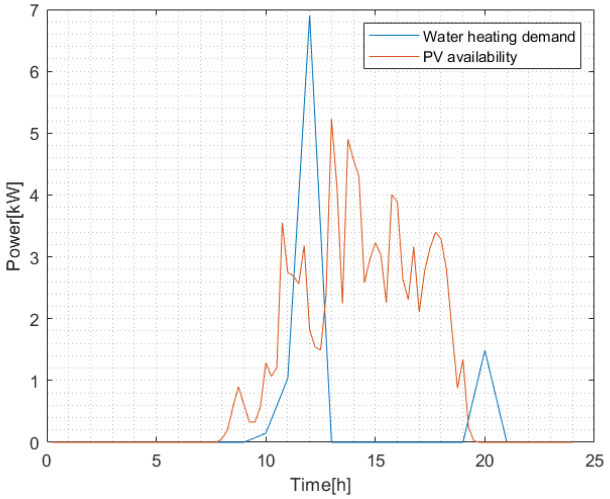

Figure 38 Demand of electricity of the electrolyser for water heating on April 15th.

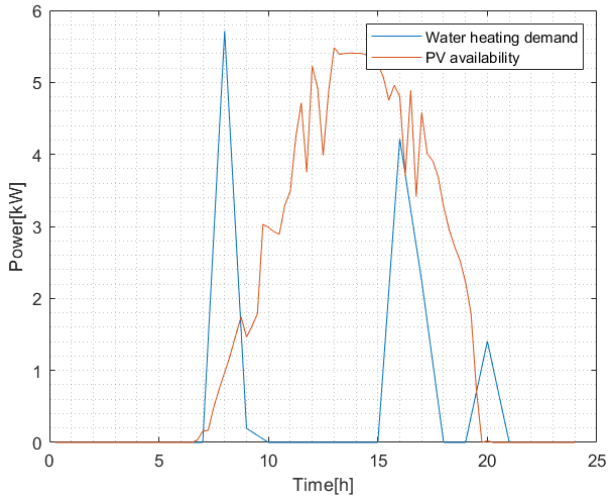

Figure 39 Demand of electricity of the electrolyser for water heating on July 21st.

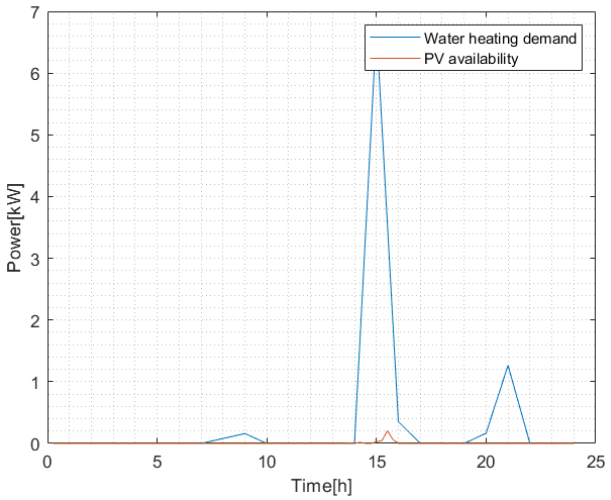

Figure 40 Demand of electricity of the electrolyser for water heating on November 21st.

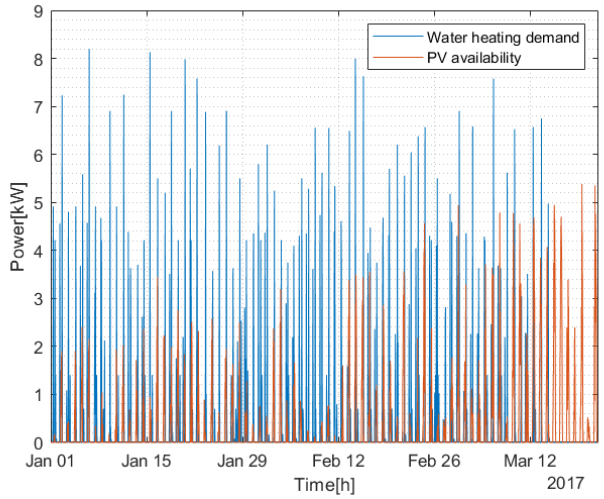

Figure 41 Demand of electricity of the electrolyser for water heating in winter.

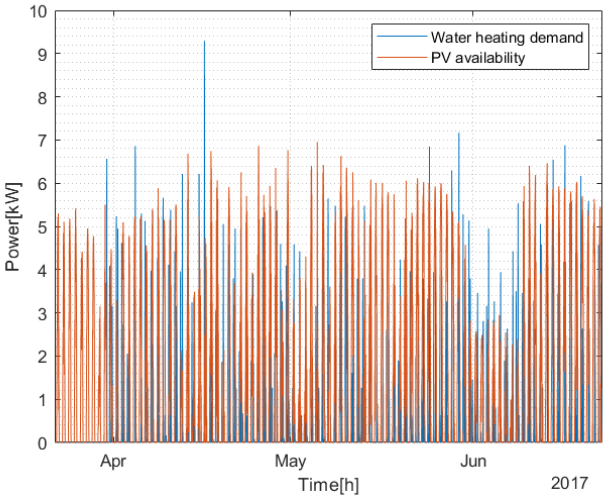

Figure 42 Demand of electricity of the electrolyser for water heating in spring.

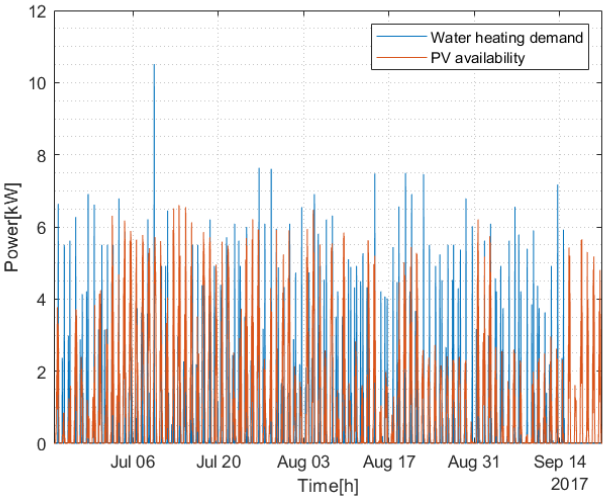

Figure 43 Demand of electricity of the electrolyser for water heating in summer.

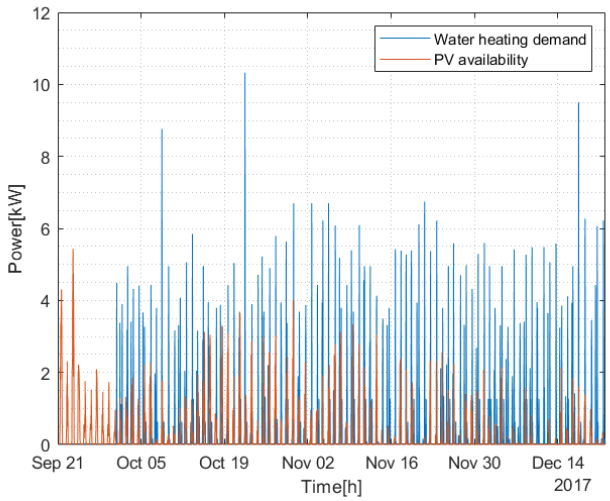

Figure 44 Demand of electricity of the electrolyser for water heating in autumn.

The plots show the mismatch between the demand of electricity to produce the hydrogen that will satisfy the domestic hot water demand, and the electricity from photovoltaic available, supposing that the appliances and lighting need is satisfied by the PV panels, when the energy is produced.

The hydrogen highest production is in summer, and in spring, which are also the seasons in which the demand for hydrogen is the lowest. Therefore, it can be interesting to implement a solution of seasonal storage, using the hydrogen as energy vector. The simulations obtained from the model run will be useful to understand if the network can have the role of storage: in fact, in big natural

gas transport systems, beyond underground gas storage, the network pipelines' volume is used to store the gas, especially in summer, to ensure the provision in winter. The simulations, collected in the next chapter will show if the same logic can be applied to small distribution systems, managing hydrogen instead of natural gas.

If the line packing is not possible, and the production of hydrogen overcomes the consumption, it would be necessary to guarantee a storage tank. It is normally not sufficient to design the storage according to the maximum hydrogen produced in a day, because the hydrogen production could have exceeded the consumption in the days before. A possible way to account for the past production can be the cumulative curve of the overproduction: summing the mismatch of the summer days it is possible to understand the effective maximum overproduction and size the storage consequently. To keep track of the hydrogen produced and not consumed immediately, the cumulative curve of mismatch of production is computed, according to the following formula:

$$c_{t_x} = \sum_{t=1}^{t_x} m_t$$

The point of the cumulative at time t_x, c_{t_x} [kg], is calculated as the sum of all the previous mismatch of mass production m_t of every instant of time t from the beginning until the current time point considered t_x. The mismatch of production is the time evolution of the difference between the production of hydrogen and its consumption. The set of mismatch data imported is in kg/s, with a frequency of 15 minutes, so the mass of hydrogen m_t must be calculated multiplying by the time step of the evolution. The yearly cumulative calculated considering only the hydrogen needed to heat up the water for sanitary purposes is in figure 45.

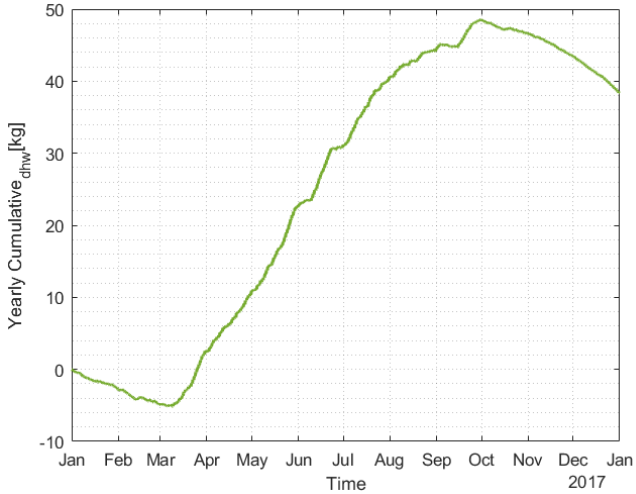

Figure 45 Yearly cumulative of mismatch of production and demand for domestic hot water supply.

The cumulative of the mismatches between hydrogen total production and hydrogen consumption for domestic water heating has an almost constant trend during the first three months of the year, then it shows a steep increase in the central months, from half of April until the end of September, and then a slight decrease in the last months of the year. The domestic hot water demand is not really dependent from the moment of the year, it is not changing much from season to season, so the steep increase during the spring and summer months is due to the increase in the hydrogen production from electrolysers, fed by solar energy. The curve confirms that the production of hydrogen in summer is sufficient to cover only the domestic hot water heating need.

5. Simulations and results

The model is run implementing the topology of the real network in the inputs, according to different configurations. In order to reduce the numerical problems, the model is run separating the two levels of pressures in correspondence with the reduction valve: the network is split in two sub-nets, each one with its own level of pressure, 8bar$_g$ and 0.1 bar$_g$.

Three different case studies with increasing complexity are analysed. Firstly, the model is tested on a base case: the medium-pressure line is reduced to one inlet and one outlet, as well as the low-pressure line. In the second case, the medium-pressure line is closed in a loop and enriched with one inlet for the hydrogen tanks, and one inlet for the connection with the electrolyser. The low-pressure line remains a single pipeline, having one inlet from the medium pressure sub-net and one outlet to the PàL. In the last case study, the configuration is enlarged considering several end-users to reproduce a district supply.

The hydrogen mass consumption had to be evaluated in order to use it into the hydrogen gas network model. The calculation of the heating needs of the house, both for space heating and domestic hot water, has been useful to get the heating demand associated to the hydrogen feeding, and, passing by the lower heating value, the hydrogen volumetric and mass consumption.

The simulations are conducted on twenty-four hours, using a time resolution of one hour, and for four different days of the year 2017, one for each season: 19th February, 14th April, 21st July, 21st November, chosen as representative days for each season of the year. Gas networks have a certain capacity of storing gas, that depends on the pressure of operation, defined as line packing.

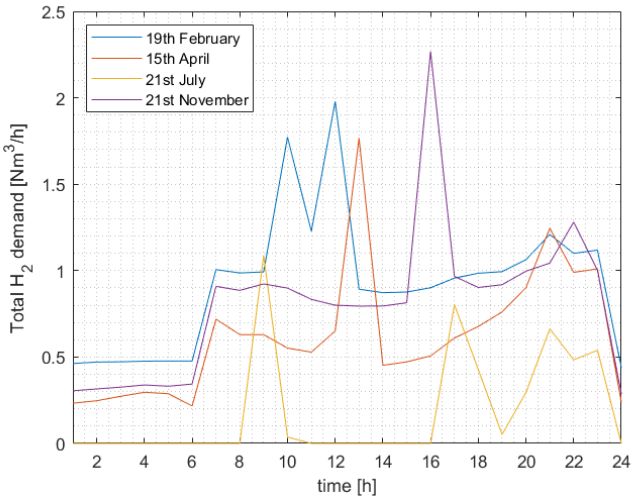

Figure 46 Volume hydrogen demand for space heating and domestic water heating for different days of different months.

The curves represent the total hydrogen required to heat up the water, both for space heating and for sanitary purposes. The domestic hot water demand is responsible for the sharp peaks of the curves, whose occurrence is quite variable during the day.

The values obtained are small, if expressed in kilograms per second they become in the order of magnitude of 10^{-5}, they represent the consumption of the Prèt-à-loger when inhabited by one person.

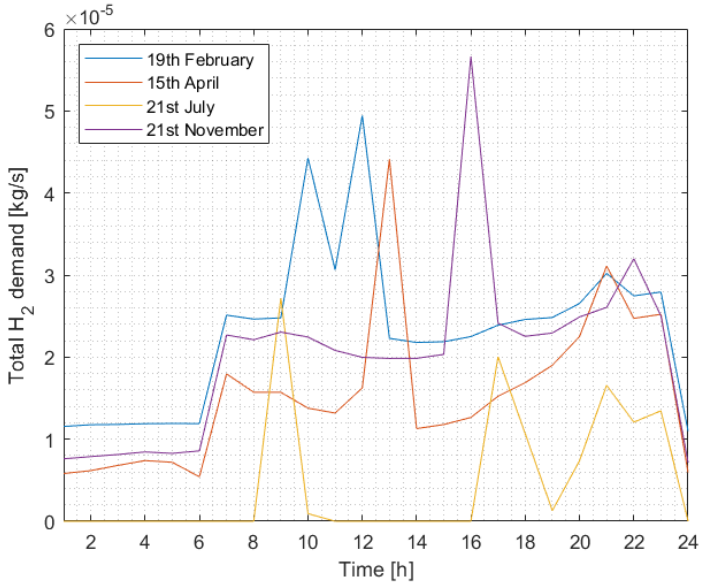

Figure 47 Mass hydrogen demand for space heating and domestic water heating for different days of different months.

The plots presented in the next chapters will show the pressure time evolution in every node, the flowrate and the line packing time behaviour in the network.

5.1 Base case

When the hydrogen is provided in pressurized tanks, the network can be reduced to a pipeline, one inlet and one outlet, both for the medium-pressure line, and for the low-pressure line. In fact, there are branches that end with nodes that are not physically connected to any end-user, so the gas velocity is virtually zero in those branches. Moreover, if the flowrate is null, the distributed pressure drop in the branch is substantially null, especially in such small distribution systems. Having the same level of pressure in two distant nodes determine numerical problems in the solving scheme. That is why the branches disconnected to end-users (and to providers as well) are not included in the simulation.

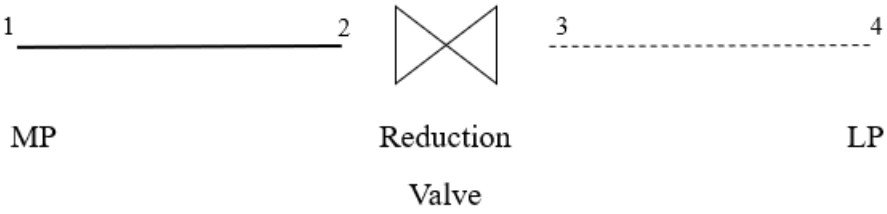

Figure 48 Base case layout.

The medium-pressure stainless steel pipeline considered in the simulation is composed of the branches 1, 2, 13 and 6 [tab. 2], representing the path made by the hydrogen gas to reach the "afleverset reductiestation", the delivery set station whose flowrate is directed to the Prèt-à-loger. The total length of the equivalent pipeline is then around 50m, while the diameter is about 50mm.

The pressure variation on the most representative day of winter (19th February 2017) and the flowrate are shown below.

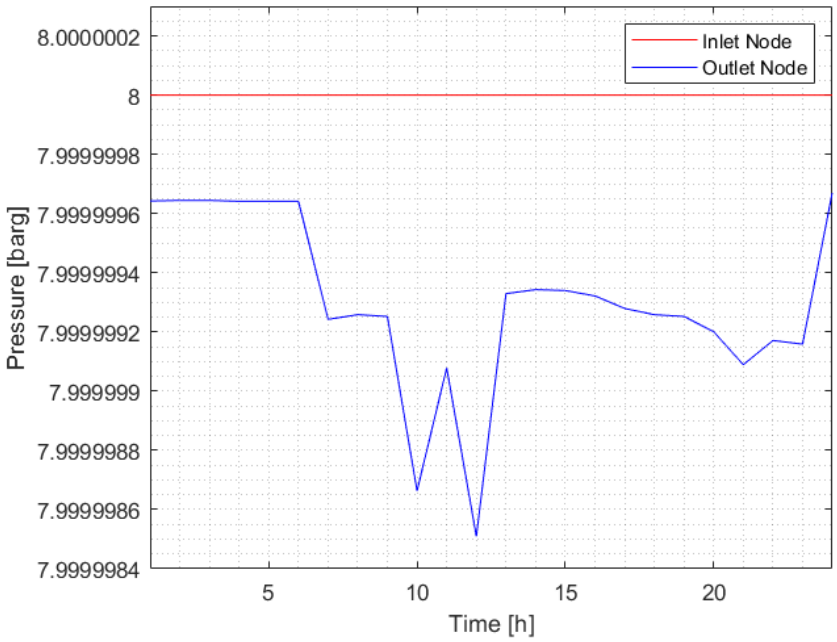

Figure 49 Pressure time evolution in the inlet and outlet node of the medium pressure pipeline on February 19th, 2017.

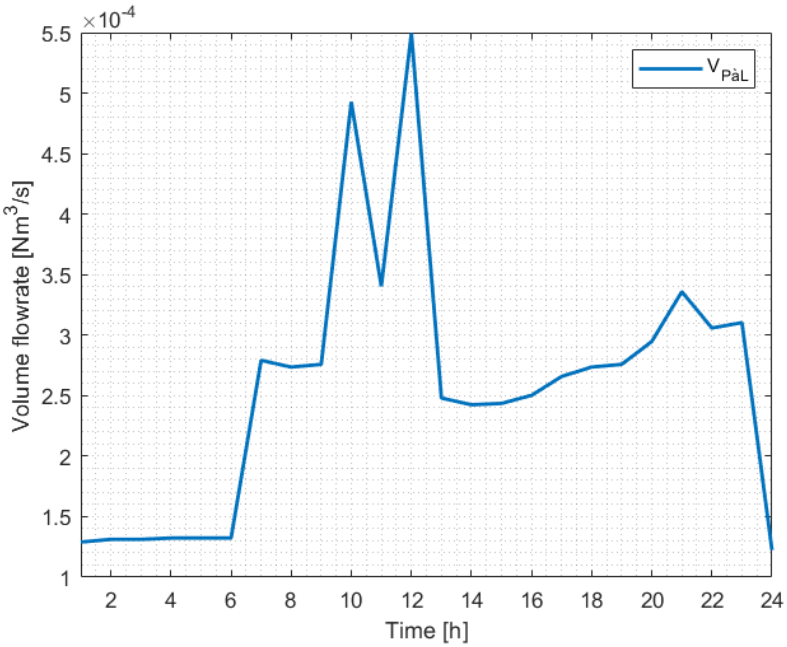

Figure 50 Hydrogen volume demand on February 19th, 2017.

The pressure change in the outlet node is very small, although consistent with the flowrate extraction: when there is a peak of demand, there is also the highest drop of pressure.

The analysis can be done also on the low-pressure line. The branches that bring the hydrogen gas to the Prèt-à-loger are the 7 and the 11 [tab. 2], for a total length of 83m. The diameters of the two pipelines are different, so the diameter for the equivalent single low-pressure pipeline is calculated as follows:

$$D_e = \frac{D_7 L_7 + D_{11} L_{11}}{L_7 + L_{11}}$$

It is a weighted average of the diameters on the lengths of the branches involved. The final value is 65mm. The value of pressure feeding, which is constant and defined by the reduction station that connects it to the medium-pressure line is around 1.1 bar. The results are shown for the different days contemporarily.

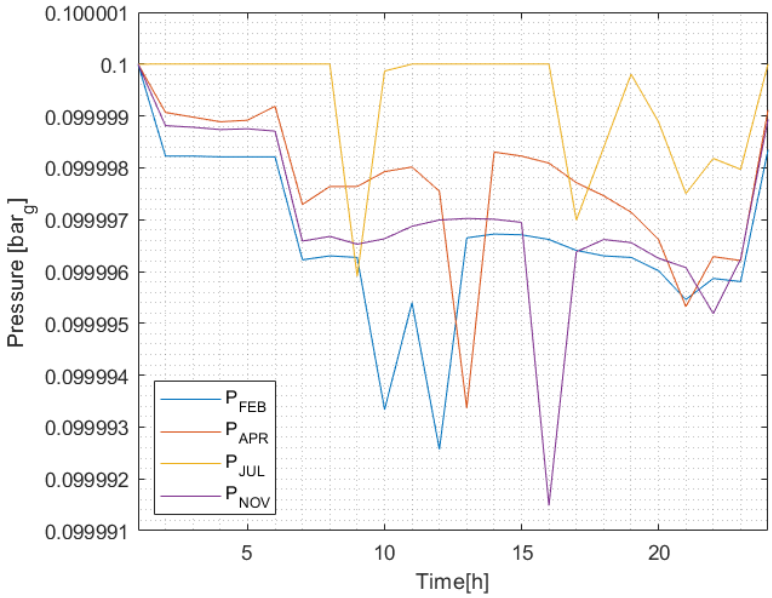

Figure 51 Pressure time evolution in different days of different months in the outlet of the low-pressure pipeline.

The pressure variation [fig. 51] is very small also in the low-pressure line, in the order of one tenth of Pascal.

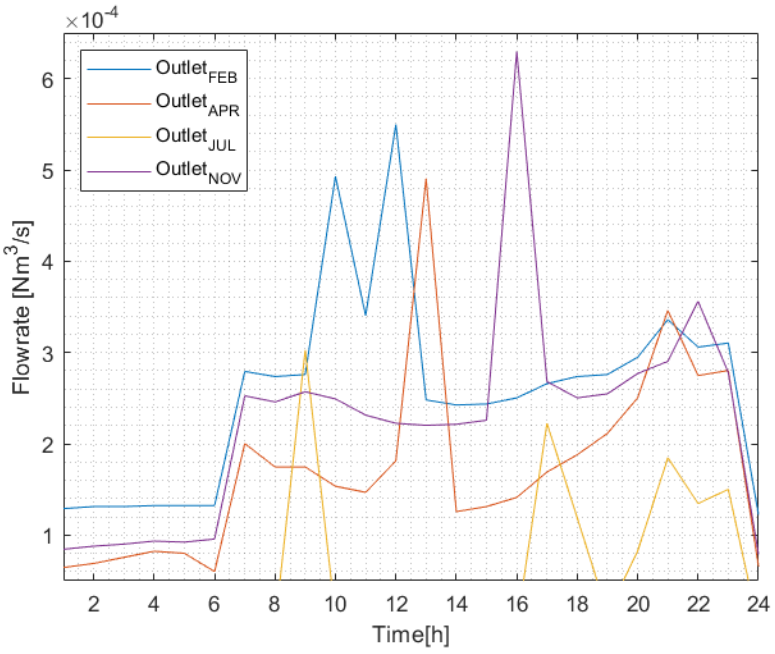

Figure 52 Hydrogen volumetric demand for domestic hot water and space heating purposes of the PàL, for different days of different months.

The volumetric demand plot [fig. 52] explains the low values of pressure drops in fig. 51, and it can be noticed as the pressure trend is specular to the flowrate trend.

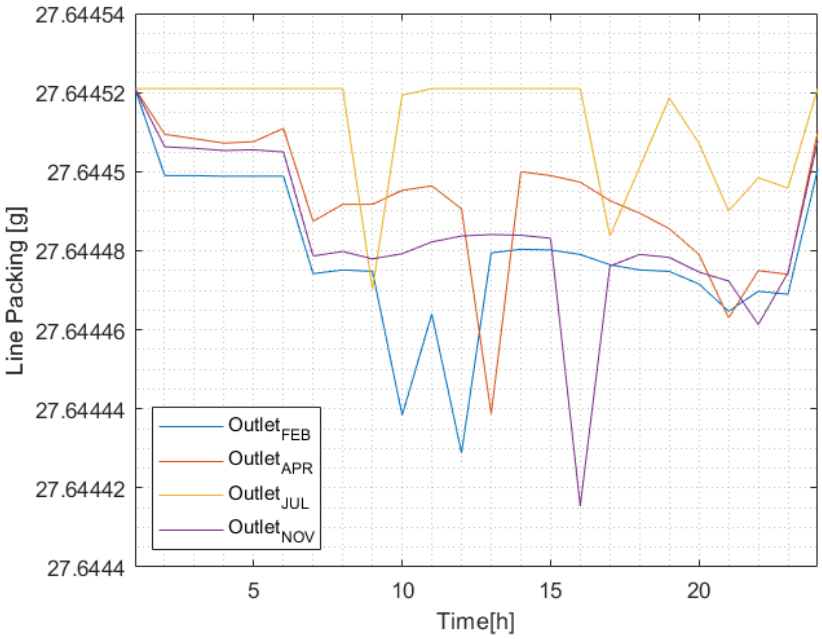

Figure 53 Line packing in the low-pressure line for different days of different months.

The line packing availability is really small for the low-pressure line [fig. 53], it is around 27.6 g, while it is more significant for the medium pressure pipeline [fig 54], about 77.4 g.

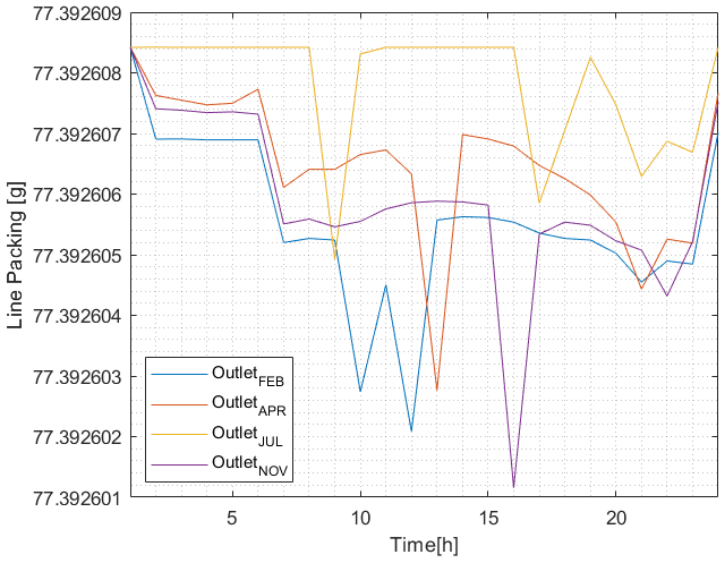

Figure 54 Line packing in the medium-pressure line for different days of different months.

In both cases, the variations are in the order of magnitude of 10^{-4} grammes.

The implementation of the single pipeline for the analysis on medium and low-pressure levels has been conducted to test the model on a simple and small system of hydrogen gas distribution. The layout configuration is slightly changed to get a system that fits better the real case.

5.2 Prèt-à-loger case

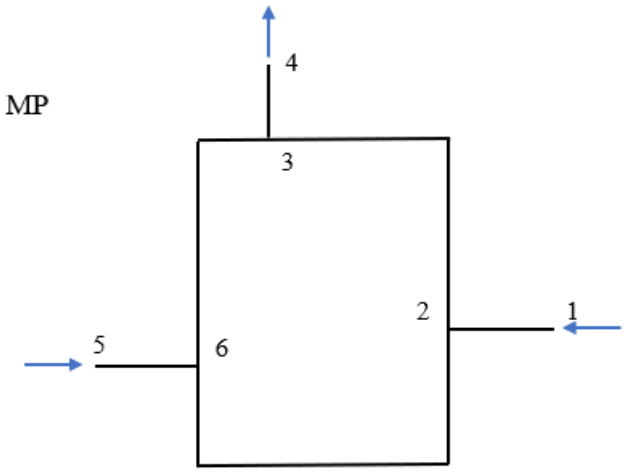

Figure 55 PàL case layout.

In this case, the hydrogen is fed not only from the tanks, but also from the electrolysers. The flowrate in the node 5, the closest to the power production and so the best option for the installation of the electrolyser, is bound to the electricity production from photovoltaic panels, and so to the presence of the sun. In order to maximize the exploitation of renewables, the electrolyser is assigned with priority of injection. The possible missing quantity of hydrogen is therefore provided by the tanks.

The simulation is run on the medium pressure line, considering the relative pressure of 8 bar_g, using the consumption data of the same four significant days used in the previous paragraphs.

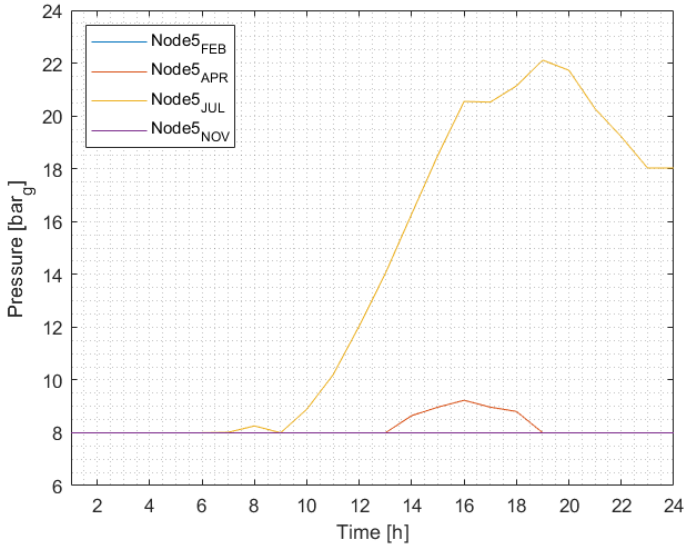

Figure 56 Pressure evolution in the electrolyser node in the medium-pressure line.

The plot shows that in the days chosen for spring (14th April) and summer (21st July) the pressure increases beyond the maximum allowed pressure of the network of 8 bar_g, reaching in summer a maximum overpressure of 22 bar_g. This is due to the fact that the hydrogen production in the days of those seasons exceeds its consumption, thanks to longer and less cloudy days and to warm weather that allows the space heating reduction (or switch off), producing a rise of pressure in the node of the electrolyser.

The day of summer considered represent an extreme situation of high production compared to consumption that can occur several times during summer. Therefore, a storage tank solution should be evaluated to keep the system safe in case of electrolyser's use, and to avoid the interruption of hydrogen production. The summer cumulative of mismatches between hydrogen production and total consumption when the only user is the PàL is positive, so the maximum value reached in terms of kg is picked, and the volume of the tank can be calculated.

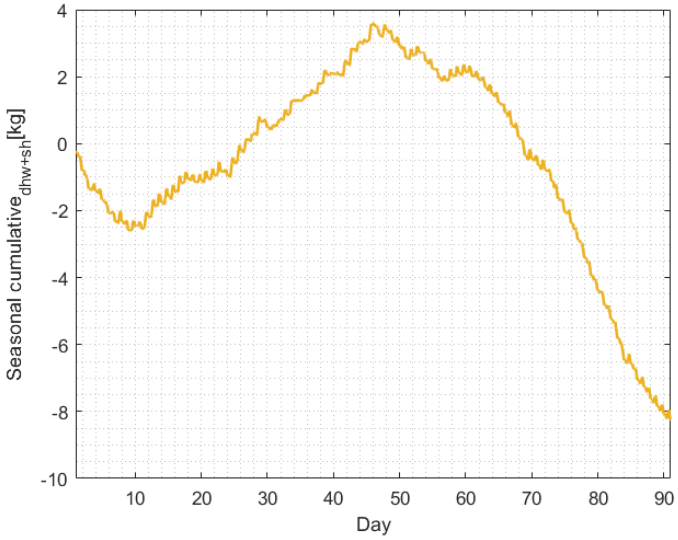

Figure 57 Cumulative of mismatch between production and consumption in summer 2017.

The cumulative computed only for summer has a maximum of 3.6 kg. The possible size V [m^3] of the storage, considering a mass of hydrogen of 4 kg, an ambient temperature of 15°C (T_2), a pressure of 9 bar (p_2), having a density at normal conditions (ρ_1, T_1=0°C, p_1=1,01325 bar):

$$V = \frac{M}{\rho_2} = \frac{M}{\rho_1 * \frac{p_2}{p_1} * \frac{T_1}{T_2}} = 5.3\ m^3$$

This is a rough estimate of the storage capacity, whose determination goes beyond the scope of this thesis.

In spring, the maximum overpressure is around 1 bar like it is possible to see from fig. 56, so there is the possibility to exploit the volume of the pipelines. In fact, reducing the pressure of operation of the network, it is possible to store the hydrogen inside the pipelines without overcoming the pressure structural threshold. Considering that the low-pressure line is working at 0.1 bar_g, the range of pressure that is allowed to exploit the line pack goes from 0.1 bar_g to 8 bar_g, so 7.9 bar of variation possible.

The pressure and line packing variations in winter and autumn days cannot be appreciated in the plot, because they are too small.

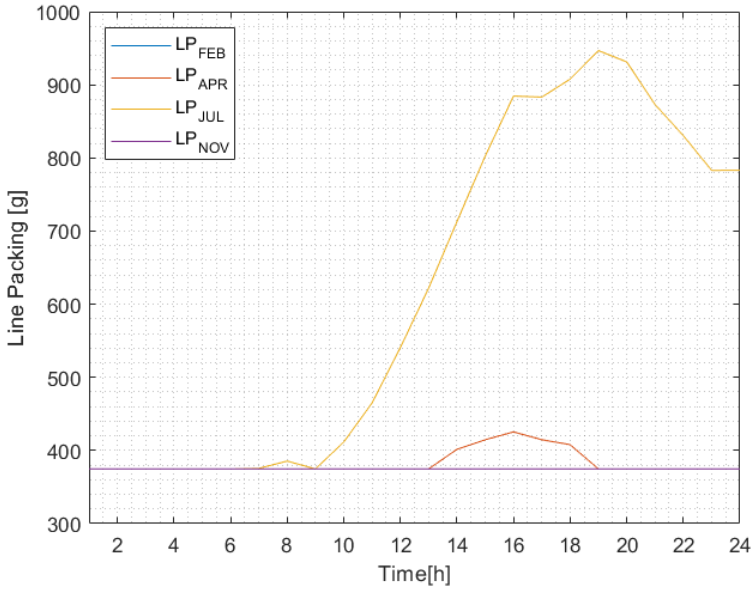

Figure 58 Line packing in the medium-pressure line for different days of different months.

Low-pressure simulation for the Prèt-à-loger is not represented, since the layout coincides with a pipeline, like in the base case.

The model is run also on a longer period in order to have a clearer picture of the pressure and line pack behaviour. It was picked a time frame of two weeks, to ensure a good graphic readability, and a modest computational cost. Since the only season in which the line packing seems possible from the daily simulations is spring, the other seasons are not considered.

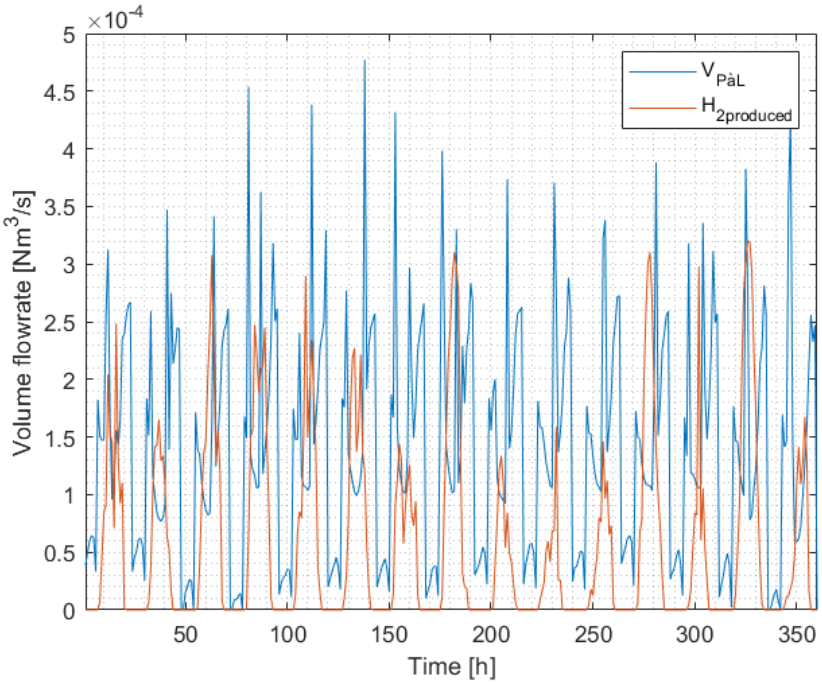

Figure 59 Hydrogen demand and production from April 23rd to May 7th, 2017

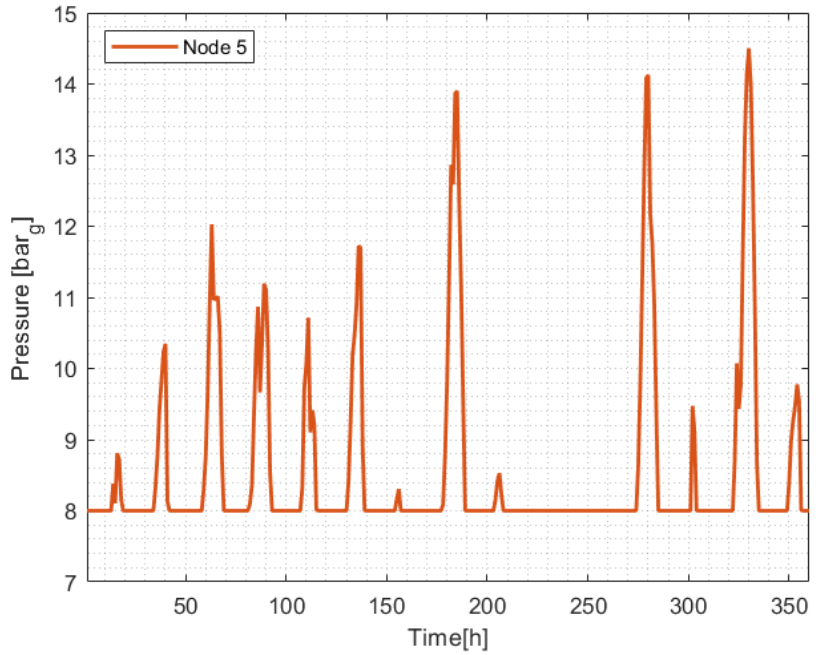

Figure 60 Pressure evolution in the electrolyser node from April 23rd to May 7th, 2017, operating pressure 8 bar_g.

In the last week of April and the first week of May, the production of hydrogen gets higher, while the consumption decreases. Consequently, the pressure in the network reaches high values. If it stays below 15.9 bar_g the line packing of the network can still be deployed. Reducing the pressure of operation, the following plot is obtained.

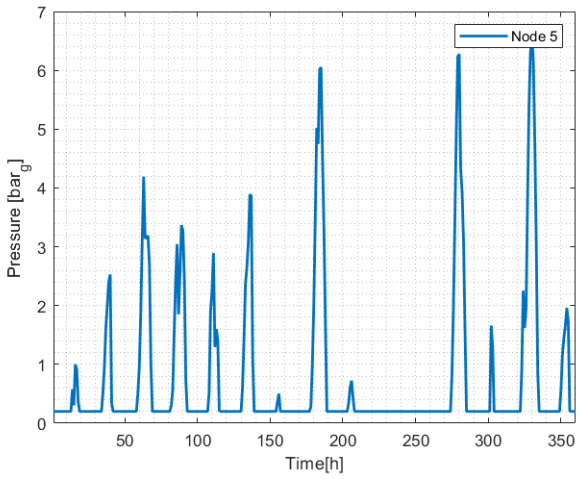

Figure 61 Pressure evolution in the electrolyser node from April 23rd to May 7th, 2017, operating pressure 0.2 bar_g

The line packing plots for 9 bar and 1.2 bar are:

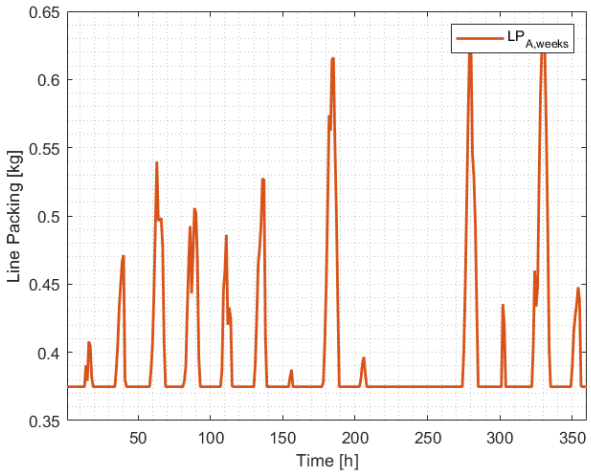

Figure 62 Line packing evolution at 8 bar_g

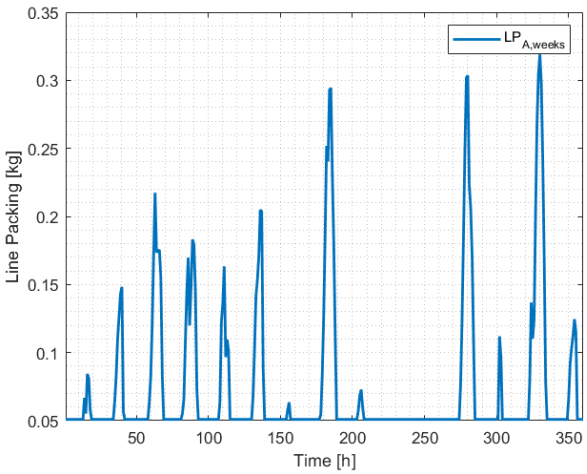

Figure 63 Line packing evolution at 0.2 bar_g

The network has been actually dimensioned to satisfy a much larger demand, further connections have been planned in the long-term horizon. The problem of the overpressure could be reduced in the case of district supply.

5.3 District case

The district configuration includes the demand of further end-users connected to the hydrogen grid. The hypothesis made to build the topology is that the medium pressure loop is fed by a tank (node 1), and an electrolyser (node 3), and that it has two outlets: one is directed to the reduction station for the Prèt-à-Loger house (node 6), the other (node 8) leads the hydrogen to a reduction station that

serves a group of consumers whose hydrogen demand is ten times the one of the Prèt-à-Loger. The load profile of the PàL is maintained for the group of end-users, and just intensified of ten times.

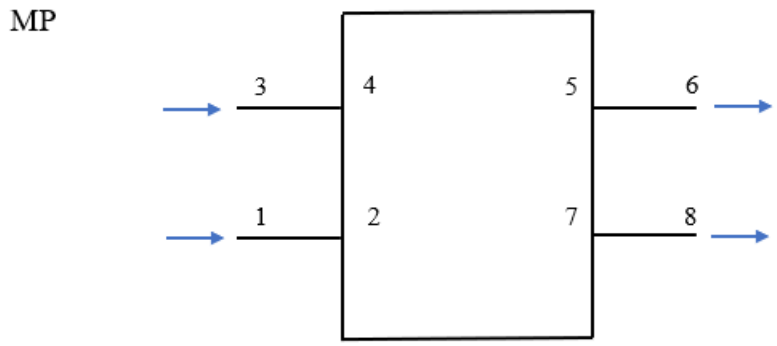

Figure 64 PàL and district case layout.

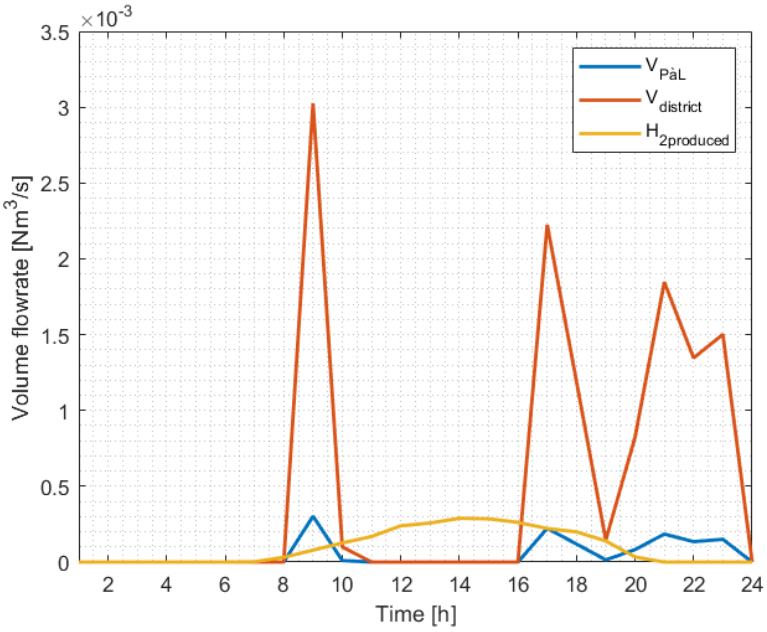

Figure 65 Demand from Prèt-à-loger and district, compared to production from electrolyser on July 21st .

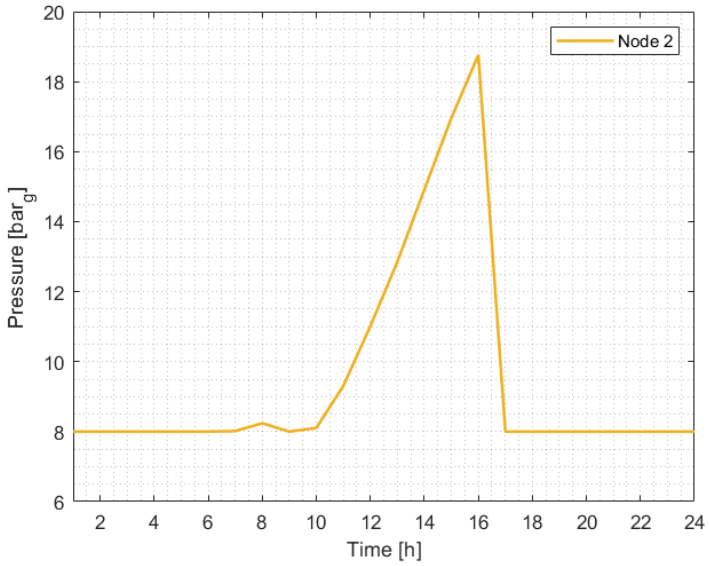

Figure 66 Pressure time evolution on July 21st in the electrolyser node of district configuration.

The pressure behaviour in the node of the electrolyser is the result of the storage of hydrogen mass inside the network during the peak production hours. Observing the flowrate plot, it is noticed that the demand in the central hours of the day is null, so the pressure in the node reaches almost 19 bar_g. The criticality observed in the simplified layout of the previous case occurs again, because the demand time profile has not changed. The maximum pressure reached in the previous case was around 22 bar_g, while in the district simulation it reduced of about 3 bar, but it is still beyond the technical constraints of the network. The line packing plot show a similar peak during the hours of maximum hydrogen production [fig. 67].

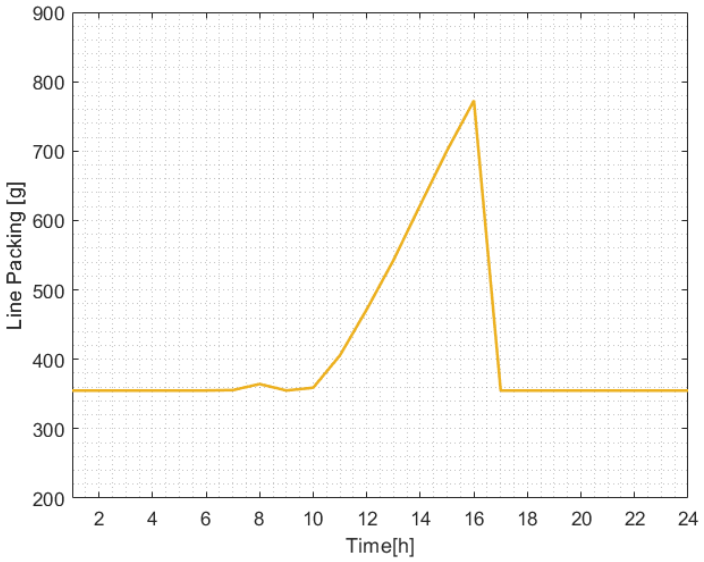

Figure 67 Line packing evolution on July 21st, 2017

Even in this case, the installation of a storage tank is necessary to guarantee the safe functioning of the network. In absence of a storage, the electrolyser should be switched off when the hydrogen production becomes too high, impeding in this way the deployment of renewable energy.

In the day of April analysed, the demand is such that all the hydrogen produced by the electrolyser is consumed. The presence of the space heating consumption is relevant during all day, so the simulation results do not show any pressure increase in the network.

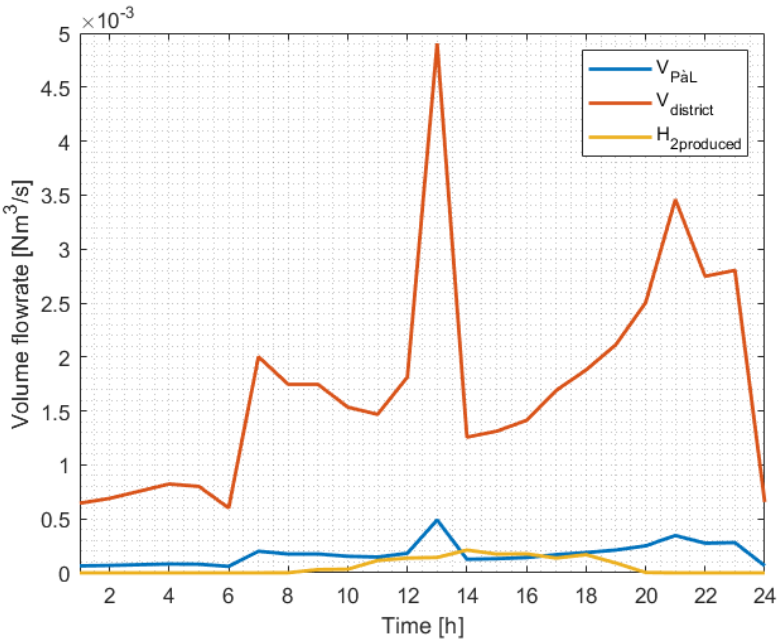

Figure 68 Volume flowrates of hydrogen produced and cosumed on April 15th

6. Conclusions

This work proposed the analysis of a case study in the Netherlands, in the Technical University of Delft, to investigate the potential of hydrogen for heating applications. First, information about the Dutch energetic and political frameworks have been collected, focusing on the projects and plans for the development of hydrogen. Then, the attention moved to the specific case of The Green Village, the area of the campus where cutting-edge technologies and systems find the opportunity to grow. That is the location of the hydrogen network experiment implemented by some Dutch energy transport and distribution operators, object of this study. The scope of the thesis was to simulate the transient behaviour of the H_2 gas network, modelled in Matlab, in different conditions, considering that the network is going to be connected to a small house (the Prèt-à-loger) in the campus during the first stage of the experimentation. Real data about the heating demand were not available, so load profiles have been generated using the degree hours method and validated with a statistic database about gas consumption supplied by and industrial partner. Since the Prèt-à-loger and the car port next to the house are equipped with solar photovoltaic panels, the opportunity of producing green hydrogen on site through an electrolyser is evaluated. Real data of power production were available for the year 2017, so they have been used to make some energy balance considerations based on the excess of electricity. The overproduction of electricity that is currently sold to the main grid can be used to feed an electrolyser and satisfy the domestic hot water heating demand of the Prèt-à-loger, while the space heating demand cannot be covered with the current installed capacity. The ability of the hydrogen of storing the renewable energy can be exploited when the hydrogen production overcomes the hydrogen consumption for heating. The model is modified to include the possibility of introducing hydrogen from an electrolyser, and it is run both in case of single connection to the PàL, and in case of larger number of end-users. When the mismatch between hydrogen production and consumption is positive, the volume of the network pipelines is used to store the gas. The simulations can predict the moments of the year when the pressure overcomes the structural pressure limits of the system. In the single connection configuration (Prèt-à-loger case), the pressure exceeds the threshold during the spring and summer days considered for the simulation. The spring season allows the line packing, if the pressure of operation of the medium-pressure line is reduced from 8 bar_g to 0.2 bar_g, while in summer it would be necessary to include a pressurized storage tank of 5.3 m^3 to maximize the self-consumption of renewable energy produced. In the district configuration, the consumption of hydrogen in spring would be so high that there would be no overproduction of hydrogen, with the current PV capacity.

In summer, because of the absence of space heating, both in PàL and in district configuration, the overpressure would be again unacceptable for the safe functioning of the network, therefore the line packing is not possible because the pressure reached results too high.

The logic employed in this work is the one applied in transport network, the results show that it is only partially applicable to distribution networks. The pipelines alone cannot work as seasonal storage for the hydrogen produced in summer in such small systems.

References

[1] "The Future of Hydrogen The Future of Hydrogen," no. June, 2019.

[2] "Hydrogenics." [Online]. Available: https://www.hydrogenics.com/technology-resources/videos/.

[3] "New Energy Coalition joins the Hydrogen Coalition - New Energy Coalition." [Online]. Available: https://newenergycoalition.org/new-energy-coalition-joins-the-hydrogen-coalition/.

[4] De Waterstof Coalitie, "Waterstof Essentiële Bouwsteen Energietransitie Manifest Waterstof Coalitie," pp. 1–8, 2018.

[5] J. Gigler and M. Weeda, "Outlines of a Hydrogen Roadmap," *TKI Nieuw Gas*, pp. 1–105, 2018.

[6] "Statistics | Netherlands - Total Primary Energy Supply (TPES) by source (chart)." [Online]. Available: https://www.iea.org/statistics/?country=NETHLAND&year=2016&category=Energy supply&indicator=TPESbySource&mode=chart&dataTable=BALANCES.

[7] "CO2 emissions (kt) | Data." [Online]. Available: https://data.worldbank.org/indicator/EN.ATM.CO2E.KT?locations=NL.

[8] "Dutch goals within the EU | Climate change | Government.nl." [Online]. Available: https://www.government.nl/topics/climate-change/eu-policy.

[9] "Eurostat - Tables, Graphs and Maps Interface (TGM) graph." [Online]. Available: https://ec.europa.eu/eurostat/tgm/graph.do?tab=graph&plugin=1&language=en&pcode=t2020_31&toolbox=type.

[10] W. Van 't Hof, "NL-Ministry of Economic Affairs and Climate Policy 1 Energy transition in the Netherlands-phasing out of gas," 2018.

[11] E. Transition, "FocusPoint," no. December, 2017.

[12] "EU Emissions Trading System (EU ETS) | Climate Action." [Online]. Available: https://ec.europa.eu/clima/policies/ets_en.

[13] D. Hirst and M. Keep, "Commons Briefing Paper SN05927," no. 05927, 2018.

[14] “Netherlands fits its new price floor - Carbon Market Watch.” [Online]. Available: https://carbonmarketwatch.org/2018/08/21/netherlands-fits-its-new-price-floor/.

[15] “Energy companies issue joint call for EU carbon price floor – EURACTIV.com.” [Online]. Available: https://www.euractiv.com/section/energy/news/energy-companies-issue-joint-call-for-eu-carbon-price-floor/.

[16] A. (member of the N. N. I. B. van Wijk, “The Green Hydrogen Economy in the Northern Netherlands,” 2017.

[17] “Gazzetta Ufficiale.” [Online]. Available: https://www.gazzettaufficiale.it/eli/id/2018/11/05/18A07049/sg.

[18] “Idrogeno: l’Italia firma la Hydrogen Initiative.” [Online]. Available: https://www.mise.gov.it/index.php/it/194-comunicati-stampa/2038612-idrogeno-l-italia-firma-la-hydrogen-initiative.

[19] “The Green Village - Campus Development - TU Delft.” [Online]. Available: http://campusdevelopment.tudelft.nl/en/project/the-green-village/.

[20] A. van Wijk, “WELCOME TO THE GREEN VILLAGE,” 2013.

[21] TU Delft Solar Decathlon student Team, “Project Manual,” no. March, 2013.

[22] W. Koppenol, “Configureren Dimensioneren gasnet en aansluitinge.pdf,” 2013.

[23] K. A. Pambour, R. Bolado-Lavin, and G. P. J. Dijkema, “An integrated transient model for simulating the operation of natural gas transport systems,” *J. Nat. Gas Sci. Eng.*, vol. 28, pp. 672–690, 2016.

[24] “PE - PolyEthylene Pipes, Flow and Pressure Loss.” [Online]. Available: https://www.engineeringtoolbox.com/pe-pipe-pressure-loss-d_619.html.

[25] “Polvalit Z PVC Pressure : Gas & Water : Products.” [Online]. Available: https://www.pipelife.nl/nl-en/products/gas/pvc_pressure_en.php.

[26] S. Pellegrino, A. Lanzini, and P. Leone, “Greening the gas network – The need for modelling the distributed injection of alternative fuels,” *Renew. Sustain. Energy Rev.*, vol. 70, no. November 2016, pp. 266–286, 2017.

[27] A. J. Osiadacz and M. Chaczykowski, “Comparison of isothermal and non-isothermal pipeline

gas flow models," vol. 81, no. June 2000, pp. 41–51, 2001.

[28] M. Chaczykowski and A. J. Osiadacz, "Comparative assessment of steady-state pipeline gas flow models," vol. 57, no. 1, pp. 23–38, 2012.

[29] M. Chaczykowski, "Sensitivity of pipeline gas flow model to the selection of the equation of state," vol. 7, no. December 2008, pp. 1596–1603, 2009.

[30] T. Ahmed and T. Ahmed, "Equations of State and Phase Equilibria," *Equations State PVT Anal.*, pp. 467–597, Jan. 2016.

[31] J. R. Travis, D. Piccioni Koch, J. Xiao, and Z. Xu, "Real-gas Equations-of-State for the GASFLOW CFD code," *Int. J. Hydrogen Energy*, vol. 38, no. 19, pp. 8132–8140, 2013.

[32] J. W. Leachman, R. T. Jacobsen, S. G. Penoncello, and E. W. Lemmon, "Fundamental equations of state for parahydrogen, normal hydrogen, and orthohydrogen," *J. Phys. Chem. Ref. Data*, vol. 38, no. 3, pp. 721–748, 2009.

[33] M. Fallahnejad, B. Eberl, and M. Günther, "Long-Term Forecast of Residential & Commercial Gas Demand in Germany."

[34] A. Kallert, R. Egelkamp, and D. Schmidt, "High Resolution Heating Load Profiles for Simulation and Analysis of Small Scale Energy Systems," *Energy Procedia*, vol. 149, pp. 122–131, Sep. 2018.

[35] D. Connolly, "Enhanced Heating and Cooling Plans to Quantify the Impact of Increased Energy Efficiency in EU Member States Work Package 2 Main Report: Executive Summary," 2016.

[36] "Energiebesparing: Een samenspel van woning en bewoner - Analy-se van de module Energie WoON 2012 | Rapport | Rijksoverheid.nl." [Online]. Available: https://www.rijksoverheid.nl/documenten/rapporten/2013/12/02/energiebesparing-een-samenspel-van-woning-en-bewoner-analy-se-van-de-module-energie-woon-2012.

[37] ECN and RIGO, "Energiebesparing: Een samenspel van woning en bewoner - Analyse van de module Energie WoON 2012," pp. 1–152, 2013.

[38] "KNMI Klimatologische Dienst - Informatie over verleden weer." [Online]. Available: http://projects.knmi.nl/klimatologie/metadata/index.html.

[39] “Beschikbare data | Liander.” [Online]. Available: https://www.liander.nl/partners/datadiensten/open-data/data.

[40] N. Pflugradt, “Modellierung von Wasser-und Energieverbräuchen in Haushalten,” no. April, p. 373, 2016.

[41] “StatLine - Energy consumption private dwellings; type of dwelling and regions.” [Online]. Available: https://opendata.cbs.nl/statline/#/CBS/en/dataset/81528ENG/table?fromstatweb.

[42] A. Honoré, *The Dutch gas market: Trials, tribulations and trends*, no. OIES Paper: NG 118. 2017.

[43] M. Santarelli, “Introduzione a Elettrolisi,” p. 20, 2018.

[44] C. Coutanceau, S. Baranton, and T. Audichon, *Hydrogen Production From Water Electrolysis*, vol. 2, no. 20. 2017.

[45] “Small and medium capacity | McPhy.” [Online]. Available: https://mcphy.com/en/our-products-and-solutions/electrolyzers/small-and-medium-capacity/.

[46] “H2data.de - Hydrogen fact sheet.” [Online]. Available: http://h2data.de/.

[47] “Good Practice Guidance and Uncertainty Management in National Greenhouse Gas Inventories CO 2 Emissions from Cement Production 175 175 CO 2 EMISSIONS FROM CEMENT PRODUCTION ACKNOWLEDGEMENTS A B S T R A C T.”

[48] R. M. Andrew, “Global CO 2 emissions from cement production, 1928-2017,” *Earth Syst. Sci. Data*, vol. 10, pp. 2213–2239, 2018.

Appendix

The electricity consumption data collected during the years 2017, 2016, 2015 are shown below. Two sensors were installed in the Prèt-à-loger: one to account for the total electricity consumption, and the other to quantify the heat pumps consumption. The charts show the inconsistency of the available data and explain why it was not possible to make use of them. The dataset is incomplete, and the heat pumps consumption is not changing seasonally.

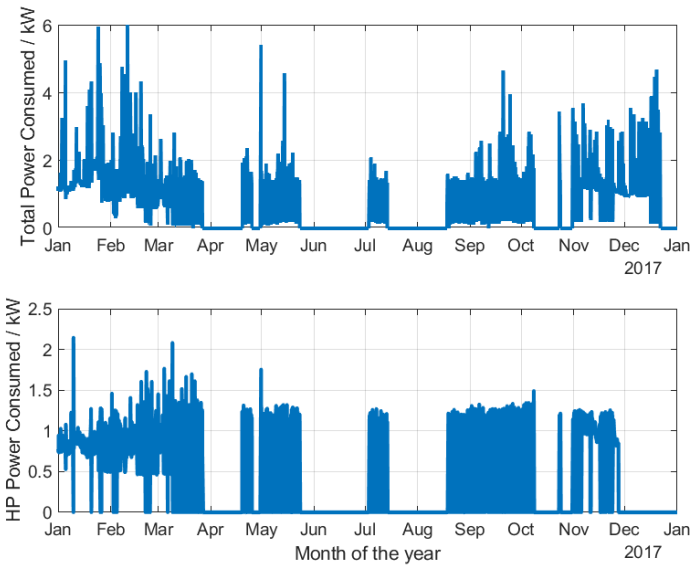

Figure 69 Total power consumption and heat pumps consumption real dataset in 2017.

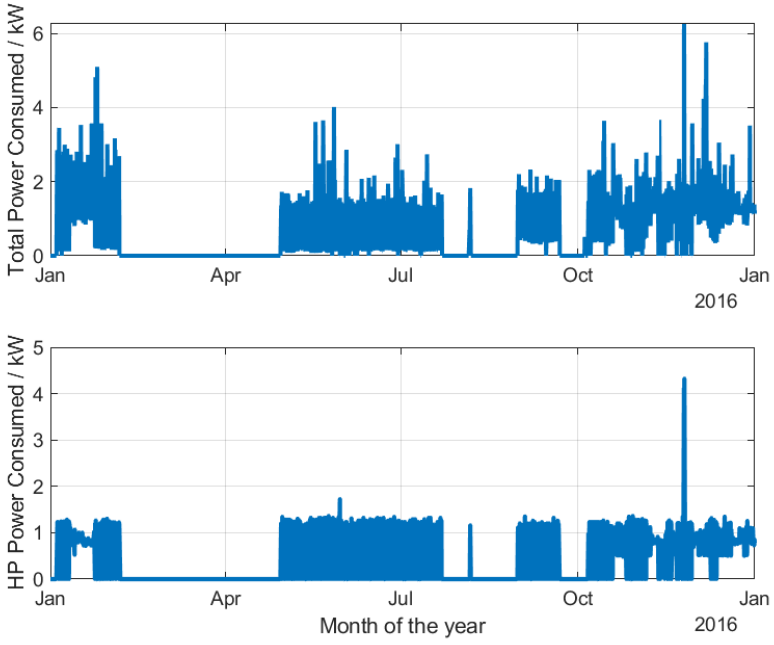

Figure 70 Total power consumption and heat pumps consumption real dataset in 2016.

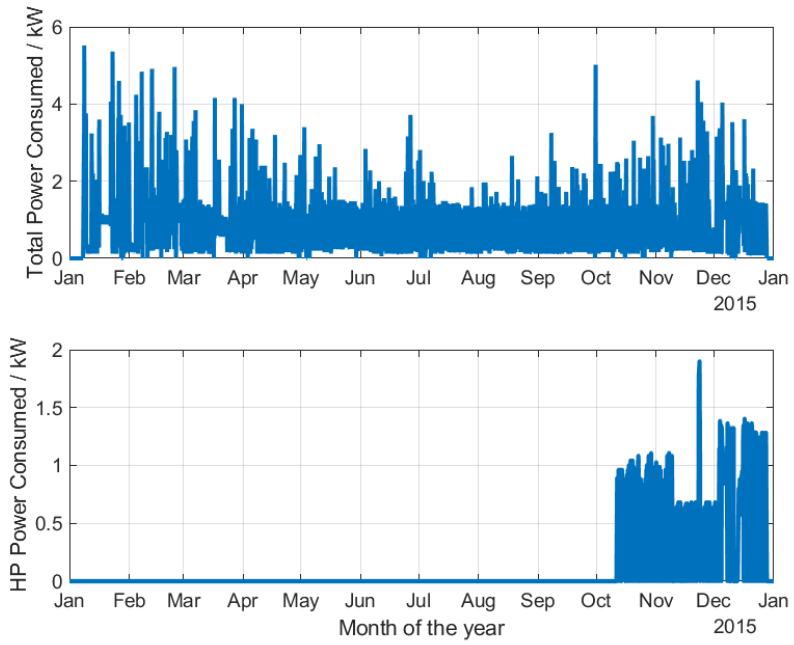

Figure 71 Total power consumption and heat pumps consumption real dataset in 2015.

In the plots below, it is shown the number of times in which a certain average daily temperature occurs, during winter, spring and autumn. This is done to pick the most significant temperature for each season, and as a consequence the days that most represent the season. The consumption data of those days have been used in the model. The analysis is not necessary in summer, because the demand in summer is just for domestic hot water, which is not depending from the outside temperature.

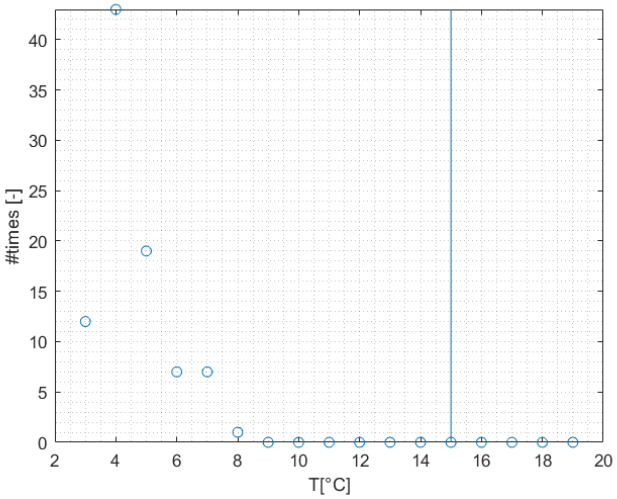

Figure 72 Frequency of average daily temperatures in Winter

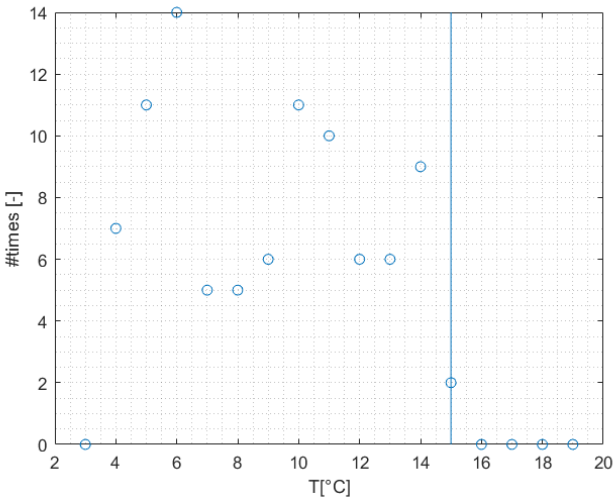

Figure 73 Frequency of average daily temperatures in Spring.

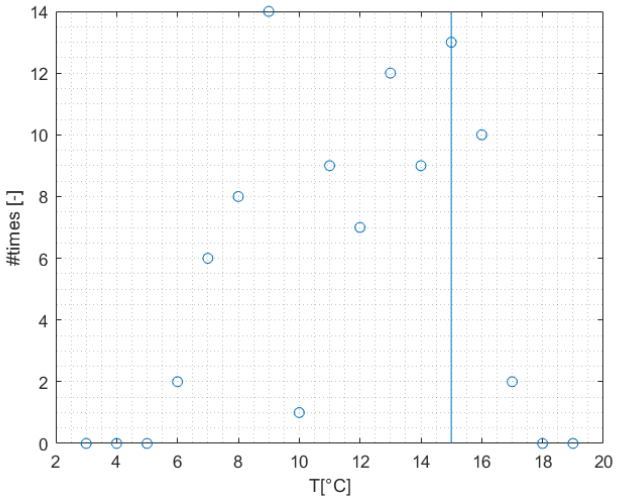

Figure 74 Frequency of average daily temperatures in Autumn.

Ringraziamenti

Questa è la parte in cui cerco di esprimere con le parole quanto sia stato importante il contributo delle persone che mi sono accanto da sempre, e delle persone che ho incontrato in questi anni.

Inizio con il ringraziare coloro senza i quali non sarei qui oggi, cioè la mia famiglia. I miei genitori, mamma Adele e papà Lorenzo, per aver creduto in me sempre, per essere il mio sostegno, la mia bussola, e il mio porto sicuro. Sono grata per il rapporto che ho con voi.

I miei fratelli. Grazie Luca, per avermi cresciuta, per avermi ispirata con la tua creatività e originalità, il tuo affetto è una certezza irrinunciabile per me. Grazie Enzo, per essere da sempre un fratello presente, che ascolta, dai principi saldi, e i consigli preziosi.

Le mie splendide cognate. Caterina, per l'affetto e la fiducia in me, per avermi rincuorato nei momenti di stress. Sara, per la dolcezza e l'affetto, per avermi ascoltata e capita.

Il piccolo grande Pietro, che mi rende ogni giorno una zia incredibilmente fiera e orgogliosa, e che mi permette di essere la sua compagna di giochi nonostante la lontananza.

Nonna Filomena, tutti gli zii paterni e materni per aver avuto parole di conforto di fronte alle mie perplessità sul futuro. I miei cugini, per il vino durante i pranzi (scusa mamma) e le risate. Un grazie speciale per nonna Rosa, esempio di forza e resilienza che non dimenticherò.

Ringrazio il mio padrino Elio, Loredana, Maria Laura e Alessandro, Emiliano, che mi hanno fatto sentire a casa in Nord Europa. Grazie per avermi accolta e coccolata.

Ci sono poi le persone che ho incontrato in questi anni da fuori sede, con le quali ho condiviso le gioie e i dolori del poli. Grazie per i pomeriggi in gruppo a finire i progetti, per le ansie condivise, il sostegno reciproco, le discussioni. Per i pranzi al punto acqua, al bar Katia (non so chi sia quella Denise), sulle scale del laib 5 e su molte altre superfici di questa università. Grazie per le tonnellate di risate durante le lezioni, i giorni non sono stati mai grigi con voi.

Grazie alle mie coinquiline, Rosanna e Ilaria, che mi hanno fatto scoprire la bellezza della convivenza, mi hanno fatto vivere con gioia gli anni della magistrale.
La fortuna ha voluto che trovassi persone speciali anche a Delft, Aurora e Alejandra, che mi sono state vicine in un momento difficile, hanno saputo comprendermi e sostenermi, rendendo l'esperienza all'estero ancora più ricca e indimenticabile.

Grazie alle mie amiche di Torino. Marianna, emiliana di nascita ma abruzzese nel cuore, la cui amicizia è stata preziosa fin dal primo anno di università. Giulia, che un'atomica bionda mi ha fatto incontrare poco più di un anno fa. Grazie per essere stata un'amica autentica, comprensiva e saggia.

Grazie a Salvatore, per le esperienze e i sentimenti che abbiamo condiviso insieme.